Title

Mechanical analysis of controls on strain partitioning in the Himalayas of central Nepal

Journal

Journal of Geophysical Research, 116(B10)

ISSN

0148-0227

Authors

Godard, V

Burbank, DW

Publication Date

2011

DOI

10.1029/2011jb008272

Peer reviewed

Mechanical analysis of controls on strain partitioning in the Himalayas of central Nepal

V. Godard[1,2] and D. W. Burbank[2]

Received 29 January 2011; revised 20 June 2011; accepted 7 July 2011; published 7 October 2011.

[1] We present a mechanical analysis of the problem of slip partitioning between the major thrust systems in a collisional range. We focus on two structures in the Himalayas of central Nepal: the Main Himalayan Thrust (MHT) and the Main Central Thrust (MCT). We use finite element modeling to test the influence of various parameters, such as friction coefficients and surface processes, and we investigate how they affect the distribution of deformation between these two faults. We observe that reproduction of the late Quaternary kinematic pattern across the range with our model requires strict conditions on the friction coefficients, such that the MHT is very weak, whereas the MCT is significantly stronger. The most important parameter that controls slip partitioning appears to be the dip angle of the MCT, with a gentler or steeper MCT promoting or inhibiting slip, respectively. We also show that transient loading and unloading through focused glacial erosion in the higher part of the range can unclamp the MCT and allow a significant increase in slip rates. The results of this mechanical sensitivity investigation have important implications for the dynamics of the Himalayan wedge and point toward along-strike structural variations as a first-order control on slip partitioning.

Citation: Godard, V., and D. W. Burbank (2011), Mechanical analysis of controls on strain partitioning in the Himalayas of central Nepal, *J. Geophys. Res.*, *116*, B10402, doi:10.1029/2011JB008272.

1. Introduction

[2] Active mountain ranges comprise rapidly evolving structural complexes whose behavior is either controlled by internal factors, e.g., lithospheric rheology, or external ones, e.g., intensity of erosion and sedimentation. One of a deforming range's most salient characteristics and probably the most important when it comes to understanding its kinematics is the existence of crustal-scale faults that accommodate a large fraction of the far-field strain. Documenting the timing and magnitude of slip that is accommodated on those individual structures has the potential to yield critical insights on the dynamics of the whole orogen [e.g., *Lavé and Avouac*, 2001; *DeCelles et al.*, 2001]. Extensive studies have been carried out in the major mountain ranges around the globe and, in many settings, have yielded a relatively thorough documentation concerning (1) the architecture of the range [*Martin et al.*, 2005], (2) the boundary conditions to which it is submitted, e.g., the magnitude of erosion and far-field long-term velocities [*Bettinelli et al.*, 2008], and (3) its internal deformation pattern [*Le Fort*, 1975; *Schelling and Arita*, 1991; *Harrison et al.*, 1998; *Hodges*, 2000; *DeCelles et al.*, 2001; *Avouac*, 2003; *Robert et al.*, 2009]. A process-based understanding of the dynamics of those orogenic systems that links all the observations mentioned above is an attractive research objective and lies at the core of numerous studies. However, a mountain range's actual physical behavior, which directly controls the way applied boundary conditions are converted into an observed deformation pattern, is still poorly understood. In particular, the mechanical principles for the partitioning of deformation across multiple fault systems are still largely unresolved, largely because of the difficulties of investigating changing fault behavior over different timescales [*Friedrich et al.*, 2003].

[3] With respect to orogenic processes, a key result of the last two decades of research is the conceptual development of the idea of interactions and couplings between tectonics and surface processes [*Beaumont et al.*, 1992; *Avouac and Burov*, 1996; *Willett*, 1999; *Thiede et al.*, 2004; *Whipple and Meade*, 2006; *Tomkin and Roe*, 2007; *Berger et al.*, 2008; *Whipple*, 2009]. Although the primary factors controlling strain patterns in mountain ranges were widely recognized to be the rheology of the lithosphere, fault strength or the characteristics of the far-field kinematic forcing, several studies have concluded that surface processes could also focus deformation in regions of high erosion and, as a consequence, control the strain pattern of the whole orogen [*Willett*, 1999]. Those surface processes actually encompass a wide spectrum of phenomena ranging from various modes of large-scale erosion [*Beaumont et al.*, 2001] to the filling of peri-orogenic sedimentary basins [*Fuller et al.*, 2006] or the growth and retreat of ice bodies

[1] CEREGE, CNRS, UMR 6635, Aix-Marseille Université, Aix-en-Provence, France.
[2] Earth Research Institute, University of California, Santa Barbara, California, USA.

0148-0227/11/2011JB008272

[*Hampel et al.*, 2007]. These processes nevertheless share a common mechanical implication which is to add or remove mass within the range and, as a consequence, to significantly perturb the crustal stress field. A particularly important previous result has been the numerical prediction that such surface processes can not only influence the large-scale and long-term deformation of mountain ranges, but that they also have the potential to modulate the slip rate of individual faults at timescales of a few thousands years [*Hetzel and Hampel*, 2005; *Hampel and Hetzel*, 2006; *Hampel et al.*, 2007; *Turpeinen et al.*, 2008; *Hampel et al.*, 2009; *Maniatis et al.*, 2009]. Such results hold first-order implications for the understanding of the partitioning in space and time of shortening between the major faults of an active orogenic wedge.

[4] The purpose of the present study is to use a mechanically based approach to investigate the factors controlling the partitioning and accommodation of deformation in an active orogenic system. Observations from the Himalaya of central Nepal underpin this exploration. The Himalayas have been a propitious site for the study of continental tectonics and geomorphology, including the investigation of potential coupling between the two, because of the intensity of climatic and kinematic gradients across the range. This range is also of particular interest for our study because kinematic reconstructions suggest that several crustal-scale thrust faults may have been sequentially active over the last few million years [*Schelling and Arita*, 1991; *Schelling*, 1992; *DeCelles et al.*, 2001; *Robinson et al.*, 2003; *Searle and Godin*, 2003; *Pearson and DeCelles*, 2005; *Leloup et al.*, 2010]. However, the mechanical rationale for the partitioning of deformation between these faults is only partially understood and is, therefore, the main question addressed by this study.

[5] First, we present the geodynamical context of the Himalayas of Central Nepal with a focus on aspects that are relevant to the specific problem of the shortening distribution between the major thrust faults. Next, we introduce the principles of the geodynamic modeling approach that we use to tackle this problem. Then, after describing the results associated with our reference model, we successively explore and discuss a range of internal parameters and external forcings that are likely to have an influence on the pattern and magnitude of deformation partitioning.

2. Tectonic Setting and Problem Statement

2.1. Overview of the Himalayas of Central Nepal

[6] We focus here on data that are specifically relevant to our study and refer the reader to published reviews for a more complete coverage of the geological and geodynamical setting of the Himalayas of Central Nepal [*Gansser*, 1964; *Le Fort*, 1975; *Hodges*, 2000; *Avouac*, 2003; *Yin*, 2006; *Avouac*, 2007]. As one of the main expressions of the ongoing collision between India and Eurasia, the Himalayan range currently accommodates ~30–50 % of the convergence between the two plates [*Bilham et al.*, 1997; *Jouanne et al.*, 1999; *Larson et al.*, 1999; *Zhang et al.*, 2004; *Bettinelli et al.*, 2006]. From a morphological point of view, the Himalayas also constitute one of the steepest topographic escarpments on Earth with a transition from near sea level in the Gangetic plain to ~5000 m on the Tibetan Plateau occurring across an horizontal distance of ~120 km.

[7] From south to north, the range comprises a distinct succession of morpho-tectonic units that are bounded by major crustal-scale, mostly contractional, structures (Figure 1). The most external unit is the Siwaliks range that is actively deforming in the hanging wall of the Main Frontal Thrust (MFT) and is overthrusting the Gangetic foreland. The MFT is currently the most active structure of the Himalayan range and, at least in parts of central Nepal, it accommodates most of the 20 mm/yr of Holocene shortening between India and southern Tibet [*Lavé and Avouac*, 2000]. The Siwaliks foothills are bounded on their northern edge by the largely inactive Main Boundary Thrust (MBT) that marks the transition to the Lesser Himalaya. Spanning from the MBT to the Main Central Thrust (MCT), the Lesser Himalaya (LH) is typified by relatively subdued topography and low rock uplift rates, and it mainly comprises metasediments of Indian affinity [*Bollinger et al.*, 2004a]. Topography starts to rise significantly when approaching a physiographic transition (PT2: [*Catlos et al.*, 2001; *Hodges et al.*, 2001; *Wobus et al.*, 2003]) and entering the metamorphic and crystalline sequence of the Higher Himalaya (HH) that lies north of the MCT and is characterized by steep hillslopes and entrenched gorges [*Pratt et al.*, 2002; *Gabet et al.*, 2004a]. Finally, the South Tibetan Detachment system separates the southern Himalayan units from the Tethyan Sedimentary Series that constitutes a large part of the high range [*Searle and Godin*, 2003]. Underlying the Lesser and Greater Himalaya and connecting with the MFT, the Main Himalayan Thrust (MHT) is considered to be the plate boundary interface along which India underthrusts the Himalayas [*Zhao et al.*, 1993; *Nabelek et al.*, 2009].

[8] Even if the MFT is the main active structure at present, the late Cenozoic history of the Himalayas is characterized by a complex sequence of southward activation and abandonment of the major structures [*Leloup et al.*, 2010]. Although the central Nepal region of the Himalayas is one of the most intensively documented mountain ranges, numerous controversies and unresolved questions concerning its geodynamical and geomorphological activity remain unresolved and lie at the core of active investigations.

2.2. Glaciations in the Himalayas of Central Nepal

[9] Glaciers are widespread in high elevation areas in the Himalayas of central Nepal and can occupy a significant fraction of the landscape above 5000 m [*Pratt-Sitaula*, 2005; *Harper and Humphrey*, 2003]. Glaciers display a wide range of variations in their present ice-discharge pattern and surface evolution along the Himalaya arc. Such variations can be related to a dual influence on their dynamics and mass balance that depends on both global northern hemisphere temperature and the intensity of the Asian monsoon. However, local geomorphic factors and, in particular, contrasts in supra-glacial debris cover also have a critical influence [*Scherler et al.*, 2011]. Few studies have attempted to document the current effective erosion that can be attributed to glaciers in the Himalayas. A local study in the Marsyandi in central Nepal catchment shows that, on average, glacial erosion rates are <10 mm/yr and are in part controlled by orographic precipitation with rates <5 mm/yr in the dry northern part of the catchment [*Godard et al.*,

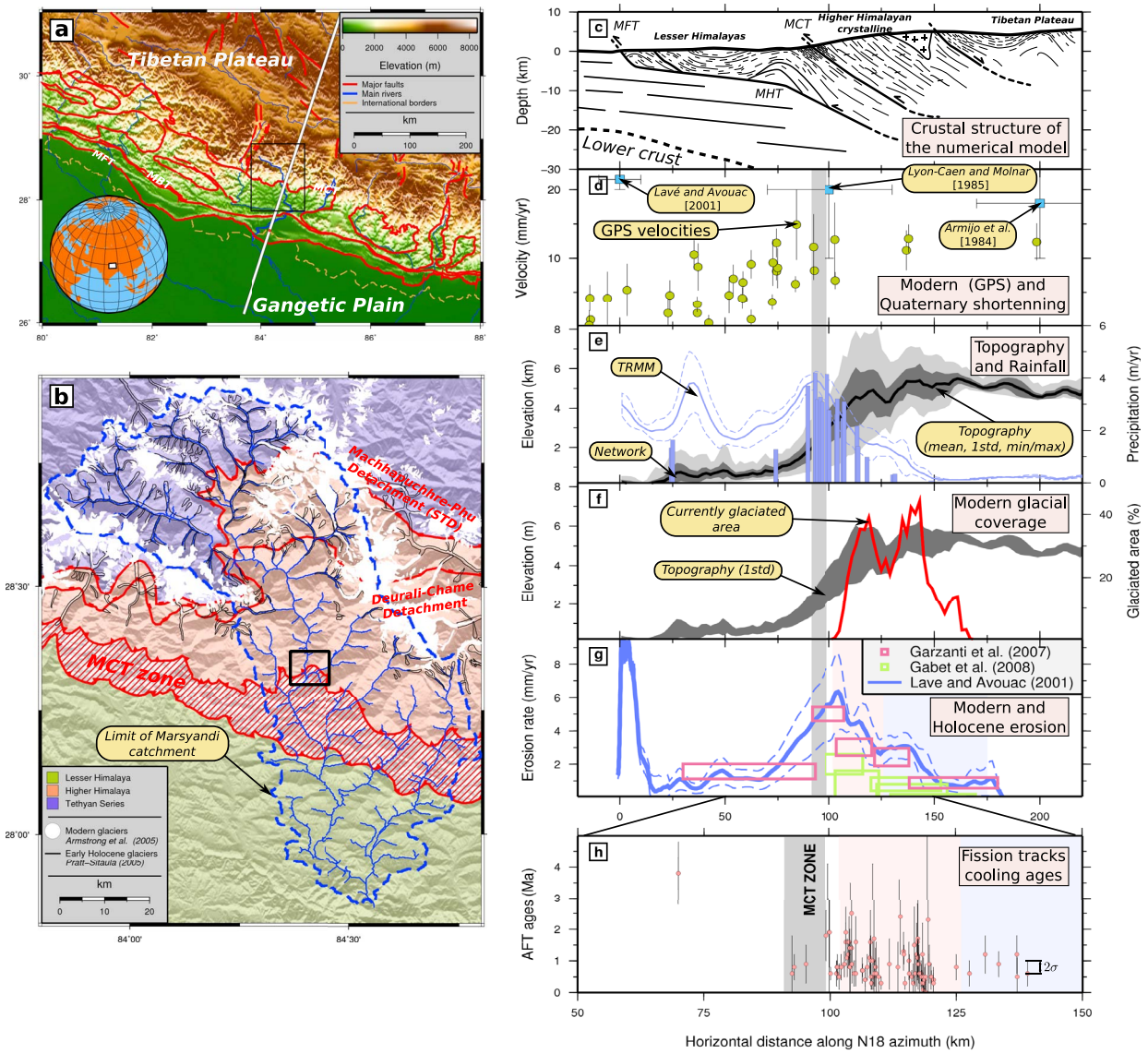

Figure 1. (a) Generalized map of the Himalayas of central Nepal, showing the position of the main faults discussed in this study. The Marsyandi catchment (black box, inset b) and the cross section used to project the data (insets c-h) are also indicated. (b) Overview map of the Marsyandi catchment in central Nepal, showing the main tectonic units [*Searle and Godin*, 2003] and modern glaciers [*Armstrong et al.*, 2005]. Black lines denote the extent of early Holocene glaciers proposed by *Pratt-Sitaula* [2005]. Black box indicates the location of Figure 2. Cross sections (N18°) across central Nepal displaying different data sets available. (c) Schematic geological cross section [*Lavé and Avouac*, 2001; *Avouac*, 2003; *Hodges et al.*, 2004] corresponding to the geometry used in the mechanical model (Figure 3). MCT: Main Central Thrusts; MFT: Main Frontal Thrust; MHT: Main Himalayan Thrust. (d) GPS velocities (circles) in a fixed India reference frame [*Bettinelli et al.*, 2006] and longer term estimates for the convergence across the Himalayas (squares: Holocene [*Lavé and Avouac*, 2000], Quaternary [*Armijo et al.*, 1986] and Late Cenozoic [*Lyon-Caen and Molnar*, 1985]). (e) Topography (mean, $\pm 1\sigma$ and extremal values) and precipitation pattern derived from TRMM data [*Bookhagen and Burbank*, 2006] and station network [*Burbank et al.*, 2003]. (f) $\pm 1\sigma$ topographic envelope (dark gray) and areal percentage of modern glacial coverage (red line) [*Armstrong et al.*, 2005]. (g) Synthetic fluvial incision profile derived from shear-stress analysis across central Nepal [*Lavé and Avouac*, 2001]. Erosion rates inferred from mineralogical spectra analysis [*Garzanti et al.*, 2007] and sediment gaging [*Gabet et al.*, 2008]. The light blue and red domains indicate the extents of two distinct geomorphic domains arising from the comparison of short- [*Gabet et al.*, 2008] and long-term [*Blythe et al.*, 2007] erosion estimates. See text for details. (h) Fission track ages in the Marsyandi catchment [*Burbank et al.*, 2003; *Huntington et al.*, 2006; *Blythe et al.*, 2007]. Note that the horizontal scale is different for this inset. Light blue and red domains are the same as in previous inset.

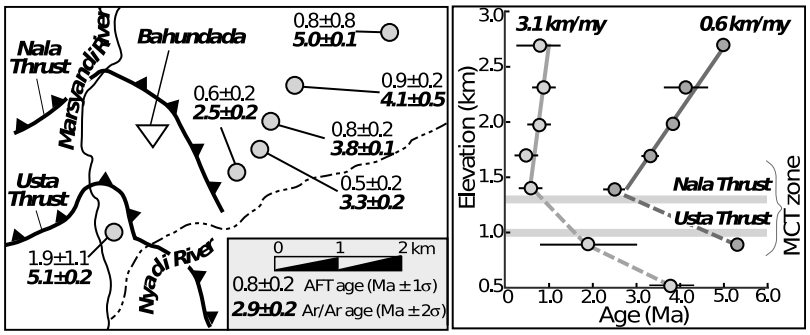

Figure 2. Sample location map and age-elevation profiles for the low-temperature thermochronology data available across the MCT zone in the Marsyandi catchment, displaying an offset in colling ages that could be a manifestation of Quaternary reactivation on related structures [*Huntington et al.*, 2006; *Blythe et al.*, 2007]. See Figure 1b for location.

2011]. Important fluctuations in the extension of Himalayan glaciers have been documented over the Quaternary [*Owen et al.*, 2002; *Owen and Benn*, 2005; *Gayer et al.*, 2006; *Owen et al.*, 2008]. In central Nepal, the depression of the Last Glacial Maximum (LGM) equilibrium line altitude (ELA) has been estimated to be between 500 and 1000 m [*Duncan et al.*, 1998; *Harper and Humphrey*, 2003; *Pratt-Sitaula*, 2005], which suggests likely changes in the relative importance of glaciers in the erosion of the Himalayan range. However, no estimates of the magnitude of past glacial erosion rates currently exist in the area, although far-field estimates suggest that the global sediment flux out of the range was significantly modulated by variations in glacial coverage [*Goodbred and Kuehl*, 1999; *Rahaman et al.*, 2009].

2.3. Two Himalayan Open Questions

[10] In Central Nepal, recent reconstructions of tectonic and erosive processes in space and time highlight two important unresolved questions: to what extent is Himalayan shortening partitioned onto faults other than the Main Frontal Thrust; and can climatically modulated variations in erosion and in both sediment and ice loading affect slip rates on major faults?

2.3.1. Quaternary Kinematic Evolution of Central Nepal

[11] Current geodetic deformation rates [*Bilham et al.*, 1997; *Larson et al.*, 1999; *Jouanne et al.*, 1999; *Zhang et al.*, 2004; *Bettinelli et al.*, 2006] and longer-term studies [*Lyon-Caen and Molnar*, 1985; *Armijo et al.*, 1986; *DeCelles et al.*, 2001] indicate that shortening across the central Himalayas in Nepal is ~2 cm/yr. For the Holocene period, a study of deformed terraces at the front of the range lying south of Kathmandu showed that most, if not all, of this shortening between India and southern Tibet could be accounted for by slip on the MFT in the Himalayan foreland [*Lavé and Avouac*, 2000]. At the scale of the whole range, this observation has spurred the development of a widely recognized geodynamical and seismotectonic model for the Himalayas of central Nepal in which the MHT is the major active crustal fault and its ramp-flat structure is responsible for the observed interseismic and long-term patterns of rock uplift [*Lavé and Avouac*, 2001; *Cattin and Avouac*, 2000; *Avouac*, 2003; *Bollinger et al.*, 2004b].

[12] In contrast, west of the Kathmandu transect, recent studies have documented offsets of both apatite fission track and muscovite ^{39}Ar-^{40}Ar ages (Figure 2 [*Huntington and Hodges*, 2006; *Blythe et al.*, 2007]), as well as structural and morphological studies [*Hodges et al.*, 2004] at some locations across the MCT Zone, that suggest that a modest but significant fraction of the Indo-Tibetan convergence could have been absorbed by slip on the MCT since 2.5 Ma. Those observations have underpinned a geodynamical model of central Nepal in which out-of-sequence thrusting on the MCT significantly contributes to the kinematic budget of the range and has moved the question of a Late Cenozoic reactivation of the MCT to the center of ongoing debates [*Bollinger et al.*, 2004a; *Hodges et al.*, 2004; *Bollinger et al.*, 2004b; *Wobus et al.*, 2005; *Whipp et al.*, 2007; *Robert et al.*, 2009; *Herman et al.*, 2010a; *Robert et al.*, 2011].

[13] One possible way to reconcile these divergent observations (all slip occurs on the MFT versus significant slip on the MCT) would be to have intermittent activity on the MCT, with the last active episode being pre-Holocene [*Hodges et al.*, 2004]. Alternatively, the discrepancies between those observations and interpretations could result from significant along-strike variations in the structures of the Higher and Lesser Himalayas in central Nepal, especially as related to the complex structure of the MCT in that region and the existence of the massive, but laterally limited Kathmandu klippe (Figure 1a). In any case, a better understanding of the mechanical behavior of the Himalayan wedge has the potential to deliver critical insights on the dynamics of those different faults and the parameters that control slip partitioning across the range, which is the main purpose of the present study.

2.3.2. Time Variations of Erosion in the High Range

[14] Another pending question and interesting conundrum in the Himalayas relates to the variation of erosion in space and time over climatic timescales. Almost 20 years of extensive studies in Central Nepal, particularly in the Marsyandi catchment, have documented spatial patterns in surface processes in significant detail and across several timescales [*Lavé and Avouac*, 2001; *Burbank et al.*, 2003; *Gabet et al.*, 2004b, 2004a; *Huntington and Hodges*, 2006; *Huntington et al.*, 2006; *Brewer et al.*, 2006; *Blythe et al.*, 2007; *Garzanti et al.*, 2007; *Gabet et al.*, 2008, 2010].

Table 1. Reference Rheological Parameters Used for the Visco-elasto-plastic Formulation Used in This Study[a]

	Upper Crust (dry quartzite)	Lower Crust (Maryland diabase)	Mantle (dry olivine)
Elasticity			
Young modulus, E (GPa)	50	50	150
Poisson's ratio, ν	0.25	0.25	0.25
Density, ρ (kg/m^3)	2900	2900	3300
Plasticity			
Cohesion, c (MPa)	10	10	10
Internal friction angle, ϕ	30°	30°	30°
Viscosity			
Standard fluidity, γ_0 (Pa^{-n}/s)	$6.3\ 10^{-24}$	$6.31\ 10^{-20}$	$7.9\ 10^{-18}$
Power law exponent, n	2.72	3.05	3.5
Activation energy, E_a (kJ/mol)	184	276	528

[a]*Kirby* [1983], *Carter and Tsenn* [1987], *Kirby and Kronenberg* [1987] and *Tsenn and Carter* [1987].

Gradients in modern erosion rates and precipitation seem to indicate that erosion in the Himalayan rain shadow [*Bookhagen and Burbank*, 2006] is up to fivefold slower when compared to wetter areas to the south [*Garzanti et al.*, 2007; *Gabet et al.*, 2008] (Figure 1g, light blue (dry) and red (wet) domains, respectively). In contrast, an exceptionally dense data set of apatite fission track ages in the same region suggests that at $\geq 10^5$-yr timescales, erosion rates are about as fast in the currently dry region as they are where the monsoon is dominant [*Burbank et al.*, 2003; *Blythe et al.*, 2007] (Figure 1h). Given that the northern, semi-arid area hosts the majority of the glaciers today and was much more extensively glaciated in the past, it has been hypothesized that erosion in the currently more arid regions was several fold faster when glaciers were more expanded in the past and compensated for slower rates like those of today [*Gabet et al.*, 2008]. In addition, these changes are likely to be coupled to the evolution of the strength of the Indian monsoon.

[15] Recent studies that tie slip on thrust faults to glacial unloading [*Turpeinen et al.*, 2008] prompt us to examine whether rapid changes in erosion and ice loads in an area located in the hanging wall of the MCT could have had an influence on the activity of this fault, as well as whether the distribution of slip between the major Himalayan thrusts can be partially modulated at climatic timescales by the locus and rate of glacial erosion and ice loading/unloading.

[16] The two potentially related geological problems that we present here (slip partitioning and the role of climatically modulated loads) are research themes that may serve to improve our understanding of mountain building in general and Himalayan geodynamics in particular. Using those observations and open questions as a starting point, this study attempts to address some basic, but still unresolved problems about the mechanical behavior and sensitivity of the Himalayan wedge and about the controls on slip partitioning between major faults in active tectonics settings.

3. Modeling Approach

[17] Here we present the rationale of our modeling approach and the main constitutive components of the mechanical model we use. Most of the pertinent ideas have been previously presented in papers to which we refer for further discussion of the numerical approach [*Cattin and Avouac*, 2000; *Godard et al.*, 2004, 2006, 2009]. The aim of our modeling approach is not to attempt to fit a specific pattern or sequence of events for the Himalayas of central Nepal, but rather to try to gain a general understanding of the mechanical behavior and sensitivity of the orogen to different parameters and forcings. We investigate processes at a timescale of 100 ky, and our modeling is based on the available knowledge for the present structure and deformation of the range. We look at the dynamics of the range starting from specified initial conditions, and we do not investigate here the long-term evolution of the Himalayas or the emplacement of the main structures [*Beaumont et al.*, 2001], but rather focus on an instantaneous snapshot of the mechanical behavior, given a configuration that attempts to mimic the available geophysical and geological data.

3.1. Mechanical Principles and Numerical Approach

[18] The mechanical problem is solved using the finite element method with a time integration based on the dynamic relaxation algorithm [*Underwood*, 1983; *Hassani et al.*, 1997]. The rheology of the lithospheric materials is considered to be visco-elasto-plastic (Table 1). Plasticity is modeled using a Drucker-Prager formulation. Viscosity is considered to be controlled by a non-linear and thermally activated flow law:

$$\dot{\varepsilon} = \gamma_0(\sigma_1 - \sigma_3)^n e^{\frac{-E_a}{RT}}, \quad (1)$$

where $\dot{\varepsilon}$ is the strain rate, T the temperature, R the universal gas constant, and σ_1 and σ_3 are the maximum and minimum principal stresses, respectively. The controlling parameters are listed in Table 1. Classical Coulomb friction is used to simulate the evolution of the contact interfaces. We refer to earlier studies for an in-depth description of the physical laws implemented and the numerical approach used to solve the constitutive equations along with their associated stability issues [*Hassani et al.*, 1997; *Godard et al.*, 2009]. The simulation duration is 500 ky of which the first half is devoted to an initial phase of mechanical stabilization of the system. Tectonic and erosion processes are gradually introduced after this initial stabilization period. The typical time step is 0.1 year. This allows us to investigate processes at a time-scale and a resolution that are relevant for both the Holocene deformation of the range and longer term evolution over the Quaternary. Due to the relatively short time span of our simulation, we do not solve the heat equation over time: instead we use a fixed thermal field [*Henry et al.*, 1997]. One important aspect of this thermal field is that it introduces a high-temperature and low-viscosity zone under

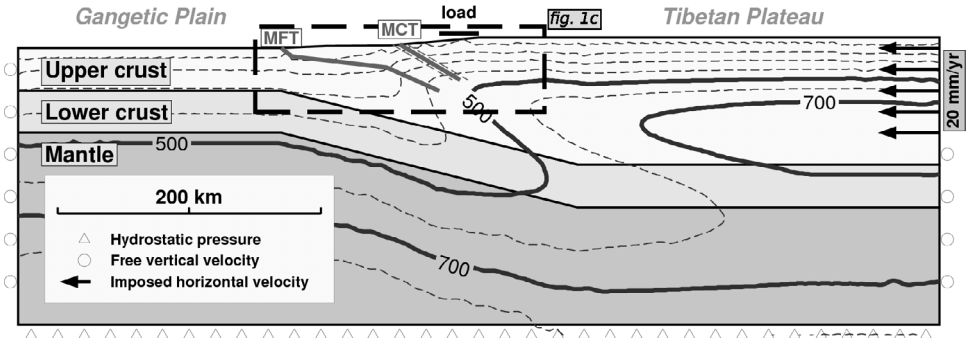

Figure 3. Structure of the mechanical model and boundary conditions used in this study. Note that the thermal field is considered static [*Henry et al.*, 1997] and that the heat equation is not solved. The thick, dark gray contours indicate the 500° and 700°C isotherms; thinner dashed contours are 100°C increment isotherms. The structure is supported by a Winkler foundation simulating isostasy. Vertical faces are permitted free vertical displacements, but no horizontal displacements. Dashed lines on both sides of the MCT indicate the laterally shifted positions of the MCT used in Figure 6. Horizontal black line denotes the portion of the topography that is subject to focused loading or unloading in Figures 8 and 9. The black dashed box indicates the position of Figure 1c.

the high range and southern Tibet that acts as a crustal-scale decoupling level and allows the transmission of the kinematic boundary conditions to the main faults (MCT and MHT).

3.2. Geometry of the Model and Boundary Conditions

[19] The general geometry of the model is similar to that used in previous works [*Cattin and Avouac*, 2000; *Godard et al.*, 2004, 2006] (Figure 3) and distinguishes between the rheological properties of the upper and lower crust [*Godard et al.*, 2004]. The geometry mimics the main features of the Himalayan orogen in central Nepal [*Zhao et al.*, 1993; *Cattin et al.*, 2001; *Hetényi et al.*, 2006; *Nabelek et al.*, 2009] and is specifically designed to match the cross section proposed by *Hodges et al.* [2004]. We use triangular elements with an average characteristic dimension of 4 km. An explicit description of the MCT as a frictional interface is a new feature in this class of Himalayan models.

[20] Vertical displacements are free, whereas horizontal displacements are set to zero on the vertical faces of the model, except for the area where a 20-mm/yr convergence velocity is applied (Figure 3). A hydrostatic foundation is introduced at the base of the model to account for isostatic support.

3.3. Erosion Formulation

[21] In order to ensure that an approximate topographic steady state condition is attained and to avoid multiplying the number of free parameters, we do not use a functional relationship to simulate background erosion [*Avouac and Burov*, 1996; *Willett*, 1999; *Godard et al.*, 2004], but rather enforce a surface condition whereby all tectonically induced rock-uplift is compensated by erosion. This constraint provides a purely kinematic definition of erosion that does not allow for full feedback mechanisms between tectonic and erosion to develop. This specification defines the background erosion acting on the topography upon which will be superimposed, for some simulations, shorter wavelength time-varying erosion to test the sensitivity of the range to unloading in specific areas. Coupled thermo-kinematic and surface evolution modeling supports the idea that the long-wavelength topography is close to steady state in central Nepal [*Herman et al.*, 2010a].

4. Slip Partitioning and Friction Coefficients

[22] Our reference model is used as a baseline against which to analyze the sensitivity to different types of perturbations. A range of friction coefficients is explored for both the MCT and MHT. Slip rates were calculated for both faults at the end of the simulation (Figures 4a and 4b).

[23] For the range of friction coefficients explored here, the system displays high variations in slip-rate values, corresponding to highly contrasting behaviors that range from most of the convergence being accommodated by the MHT for high values of the friction coefficient on the MCT and low values on the MHT, to the opposite configuration. This trade-off is a simple expression of the minimum work principle that favors the fault which is the most energetically efficient in accommodating deformation. If we consider the Holocene kinematic situation in central Nepal, in which most of the convergence appears to be accommodated by the MHT and limited slip occurs on the MCT, such slip partitioning points to the existence, in our models, of a relatively narrow range of friction coefficients for both the MHT and MCT that allows us to reproduce such observations (shaded region on Figures 4a and 4b). The current slip partitioning, therefore, implies a strong MCT ($\mu > 0.1$) that minimizes the amount of slip accommodated on it, whereas the MHT is weak ($\mu < 0.02$) such that most of the convergence occurs on this thrust. Such low values for the friction coefficient on the MHT are consistent with some estimates of the friction on major continental faults [*He and Chéry*, 2008]. We also note that, within the shaded zone (Figures 4a and 4b), the slip rates for both the MCT and MHT are highly sensitive to changes in the friction coefficient. Such gradients suggest that small variations of the friction coefficients on either the MCT and MHT could lead to significant modifications of the slip partitioning between those two faults.

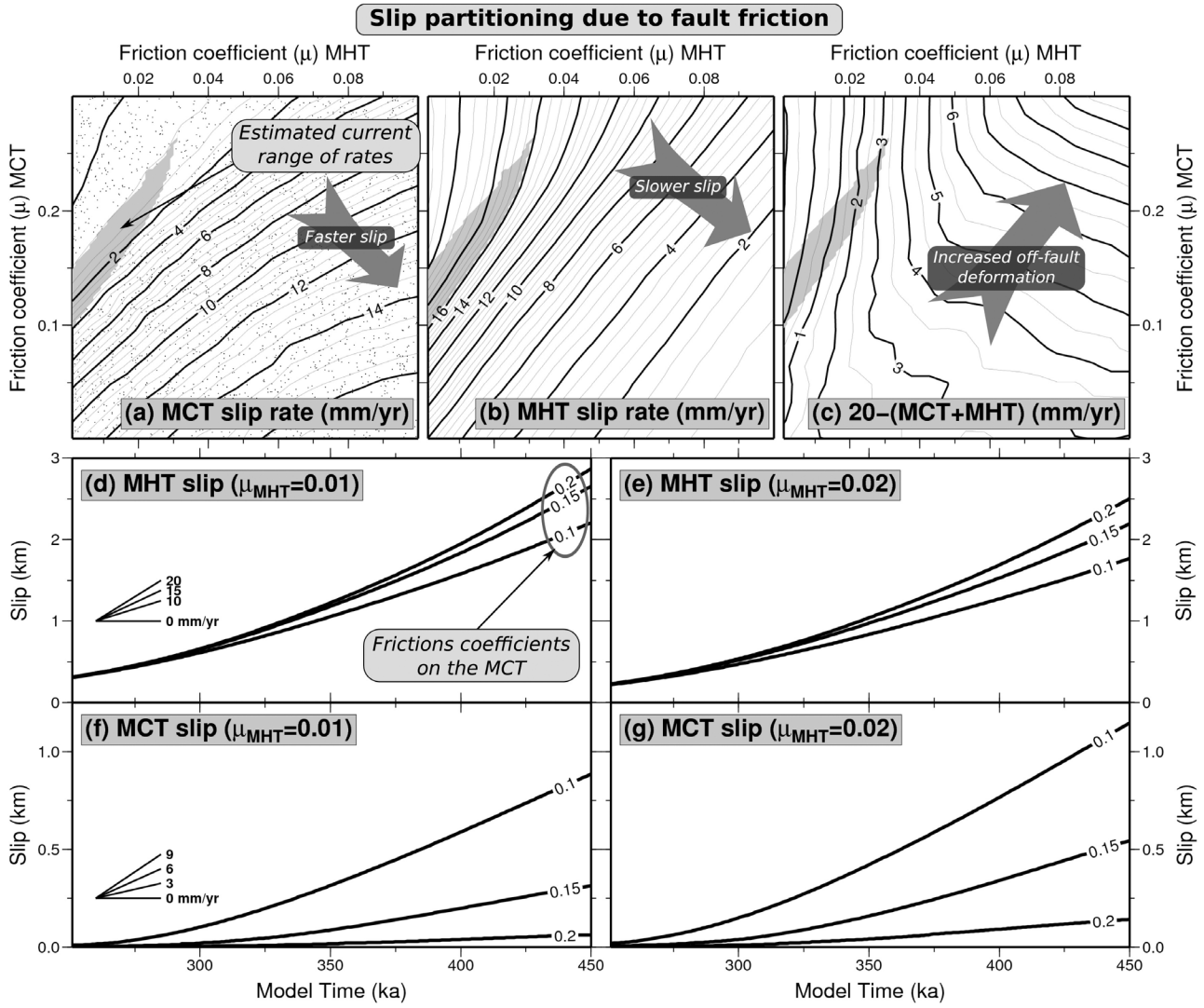

Figure 4. Exploration of the influence of different combinations of friction coefficients for the MCT and MHT in terms of slip rates on those structures. (a) Slip rate on the MCT. Light gray areas indicate the range of values for the friction coefficients that can be considered as reasonable given the Quaternary kinematic pattern in central Nepal (slip on the MCT ranges between 0.5 and 4 mm/yr and slip on the MHT is greater than 16 mm/yr). The contoured surface is derived by griding from more than 2000 individual model runs (small dots), sampled in the parameter space [*Wessel and Smith*, 1991]. (b) Slip rate on the MHT. (c) Difference between the applied velocity (20 mm/yr) and the combined slip rates on the MCT and MHT. This difference is considered as an estimate of the amount of shortening that is accommodated by distributed crustal deformation. Overall, slip rates increase on the MCT for lower friction on it and/or for higher friction on the MHT. Increasing friction on both faults leads to increased off-fault deformation. (d–g) Finite slip evolution on the MHT and MCT for selected combinations of friction coefficients.

This model response implies a potentially high sensitivity of the system to perturbations.

[24] The difference between the applied far-field convergence rate and the slip rates actually accommodated on the MCT and MHT provides an estimate of the amount of convergence that is not taken up on the MHT/MCT system, but is instead expressed as distributed strain and crustal thickening (Figure 4c). Such off-fault deformation is highest when the friction coefficients are large and thus when the mechanical resistance of the fault system as a whole is maximized. Slightly negative values for low MHT friction (Figure 4c) are indicative of a small amount of gravitational collapse of the topographic margin toward the foreland and are mainly promoted by a weak MHT. For such low friction coefficients on the MHT, the sensitivity to changes in the friction on the MCT is decreased. Such behavior is consistent with a predominance of large-scale displacement and gravitational collapse by basal sliding on the MHT, whereas the MCT has only a second-order mechanical role.

[25] For selected friction coefficients, individual time series of the finite slip on the MCT and MHT show the important role of the MCT friction in modulating the slip of

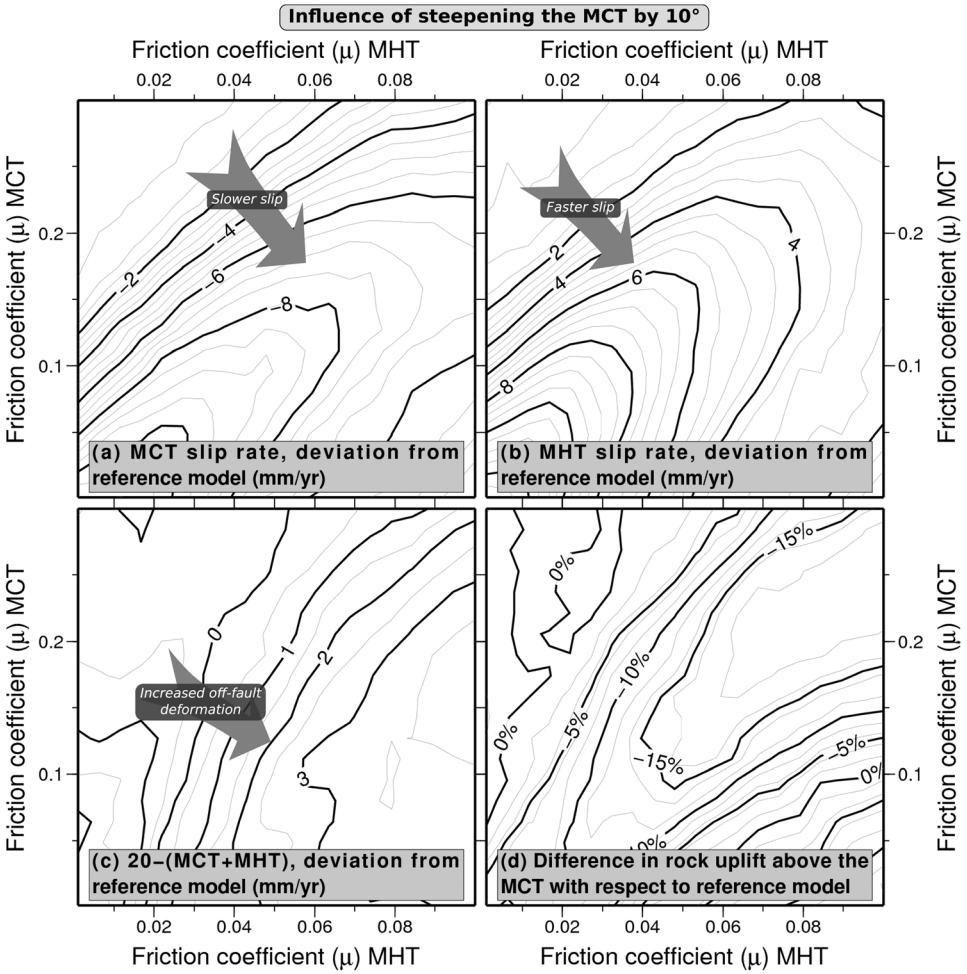

Figure 5. Influence of the dip of the MCT on the slip partitioning between the MCT and the MHT. Plotted values (mm/yr) represent the difference between a model with a steep MCT (30°) and the reference model (20° in Figure 4). (a) Difference in slip rate on the MCT with respect to the reference model (Figure 4a). (b) Difference in slip rate on the MHT with respect to the reference model (Figure 4b). (c) Difference between the applied velocity (20 mm/yr) and the combined slip rates on the MCT and MHT, with respect to the reference model (Figure 4c). (d) Difference in rock uplift rate above the MCT (in %) with respect to the reference model. Slip rates and rock uplift are highly sensitive to fault dip such that higher dips depress slip rates and promote slip transfer to gentler faults.

the whole fault system (Figures 4d–4g). Variations of the MCT friction from 0.1 to 0.2 imply a transition from a partitioning pattern where both faults have roughly equal contributions in the accommodation of deformation toward a situation of significantly suppressed slip on the MCT and dominant activity on the MHT.

5. Internal Controls on Shortening Partitioning

[26] We investigate here how some internal parameters, such as structural configuration, influence the partitioning of deformation between the MCT and MHT. Fault geometry directly influences how the ambient stress field is expressed as shear and normal stresses on the fault plane and, therefore, plays an important role in promoting or inhibiting slip. At least in some parts of the Himalayas, the MCT is a complex set of thrust faults instead of a single structure [*Hodges et al.*, 2004; *Martin et al.*, 2005; *Searle et al.*, 2008]. This network of faults and large-scale shear zones defines the MCT zone which makes the practical definition of the actual surface trace of the fault difficult. Similarly, whereas the foliation inside the MCT zone has been extensively measured, the actual dip of the fault plane itself is still poorly resolved due to the lack of sufficiently high-definition geophysical imagery. *Hodges et al.* [2004] reported dip angle values ranging from 19° to 33° for the different thrusts that they mapped in the physiographic transition (PT2) area along the Marsyandi. Other studies in central Nepal reports values of the foliation in the area affected by MCT deformation from 17° to 45°, with most observations in the 20–30° range [*DeCelles et al.*, 2001; *Hodges et al.*, 2004; *Martin et al.*, 2005; *Pearson and DeCelles*, 2005; *Martin et al.*, 2010]. Here we explore the response of the system to different changes in the configuration of the MCT for both its dip and position with respect to the High Himalayan topographic front. Given the absence

of data to indicate otherwise, we model the MCT as a planar, uniformly dipping fault surface.

5.1. Dip Angle of the MCT

[27] A striking difference in slip rate occurs between a model where the dip angle of the MCT is 30° versus the reference model where the dip angle is 20° (Figure 5). The general outcome of this sensitivity test is that a steeper angle for the MCT makes it mechanically harder to accommodate convergence on this structure and, therefore, promotes slip on the MHT. As could be intuitively expected, in a steeper configuration, a larger amount of the horizontal stress resulting from the boundary conditions is going to be expressed as normal stress on the fault plane and that stress inhibits slip. The difference with respect to the reference model is least pronounced for a combination of high friction on the MCT and low friction on the MHT. Indeed, such friction coefficients tend to drastically diminish the mechanical role of the MCT and make the system globally insensitive to changes in its geometry. Conversely, the difference with respect to the reference model is highest when friction coefficients are low for both faults (Figure 5). In this case, both faults are weak and likely to be activated. As long as frictional coefficients are low, a change toward a high dip angle on the MCT, which is mechanically unfavorable, makes the MHT comparatively much more efficient in accommodating convergence. As a consequence, when compared to the reference model, a 10° steeper MCT causes an ~10 mm/yr transfer of slip to the MHT. Increasing the friction on the MHT will tend to counterbalance this effect and progressively decrease the relative efficiency of the MHT, thereby leading to a diminishing difference with respect to the reference model.

[28] On the basis of slip rates on both faults and their respective dip angles, we calculate the rock-uplift rate above the MCT, due to the summed contributions of advection on the MCT and on the ramp of the MHT located directly below (Figure 3). We observe that, even if fault slip rates are modulated by the change in dip angle of the MCT, the actual rock uplift rate above the MCT is not significantly modified between the two models and the difference is actually less than 5% in the domain of friction coefficients that is compatible with proposed kinematic scenarios (Figure 5d). The transfer of slip from one fault to another is also associated with correlated variations of the respective contributions to rock uplift. These contributions globally compensate each other, so that total rock uplift is roughly equal between the two configurations.

5.2. Position of the MCT

[29] Given the complex of faults that constitute the "MCT zone" [*Searle and Godin*, 2003; *Hodges et al.*, 2004; *Martin et al.*, 2005], we explore the impact of slip along a more proximal or distal fault strand. In particular both the physiographic transition and faults identified by *Hodges et al.* [2004] are located south of traditionally mapped position of the MCT. Hence it is relevant to assess the differences in mechanical response in differing spatial configurations. For example, shifting the MCT north or south by ±5 km with respect to the Himalayan crest impacts the strain partitioning between the MHT and MCT, but with a lesser magnitude than variations caused by changes in dip angle (Figure 6). Deviations from the reference model are <3 mm/yr and, due to this relatively narrow range of variations, additional effects related to modifications in the distributed strain accommodation in the upper crust make the resulting total response of the system more difficult to interpret.

[30] Notably, shifting the MCT to the south by 5 km brings it closer to the ramp of the MHT, such that the stress environment of the two faults becomes more similar, thereby reducing the contrast in behavior between them (Figures 6a and 6b). Such a situation diminishes the mechanical advantage of transferring slip on the MCT when friction conditions on the MHT are less favorable. For example, for a strong MHT ($\mu > 0.05$) and a weak MCT ($\mu < 0.15$), which is a configuration where the system would tend to favor the transfer of slip toward the MCT (Figure 4), the proximity of the two faults causes the modeled slip to be lower on the MCT and larger on the MHT when compared to the reference model (Figures 6a and 6b). Similarly, when moving toward a weaker MHT and a stronger MCT, the slip on the MHT becomes progressively lower than in the reference case (up to a ~−2 mm/yr difference), whereas slip on the MCT becomes slightly faster (up to 0.25 mm/yr): changes that denote that the MCT is comparatively more efficient at accommodating slip than in the reference case. This relative efficiency is a direct expression of the diminished contrast between the two faults. The fact that contours for the 0 mm/yr difference in slip are not coincident for the MCT and MHT indicates that additional changes are predicted to occur in the relative contribution of distributed strain in the crust, as a response to the modification of the structure of the fault system. Globally, these results suggest that, in comparison to our reference model, an out-of-sequence activation of structures located progressively farther south of the current MCT becomes successively more difficult. Conversely, a northward shift of the MCT has comparatively less impact on the slip on the MHT (Figure 6d). This shift tends to induce faster and slower slip on the MCT and MHT, respectively, and thus corresponds to a situation where the contrast between the faults is amplified and the MCT appears to be slightly more efficient from a mechanical point of view. The contrast is greater when both faults are weak, which represents a situation where the global fault system is more reactive to changes in the structural configuration.

6. External Controls on Shortening Partitioning

[31] As illustrated by previous studies, variations in surface loads can modify the stress field and, thereby, have a first-order impact on the slip pattern of major faults [*Hetzel and Hampel*, 2005; *Hampel and Hetzel*, 2006; *Hampel et al.*, 2007; *Turpeinen et al.*, 2008; *Hampel et al.*, 2009; *Calais et al.*, 2010]. In our case, surface loads that can potentially affect the MCT and the MHT are related both to the temporal evolution of glaciation in the high range and to the distribution of erosion in space and time. As previously described for the Himalayas of central Nepal [*Pratt et al.*, 2002], denudation and, in particular, glacial erosion and ice loading appear to display significant variations with time in that area.

[32] Variations in surface loads modify both the normal and shear stresses acting on the fault plane. In turn, these

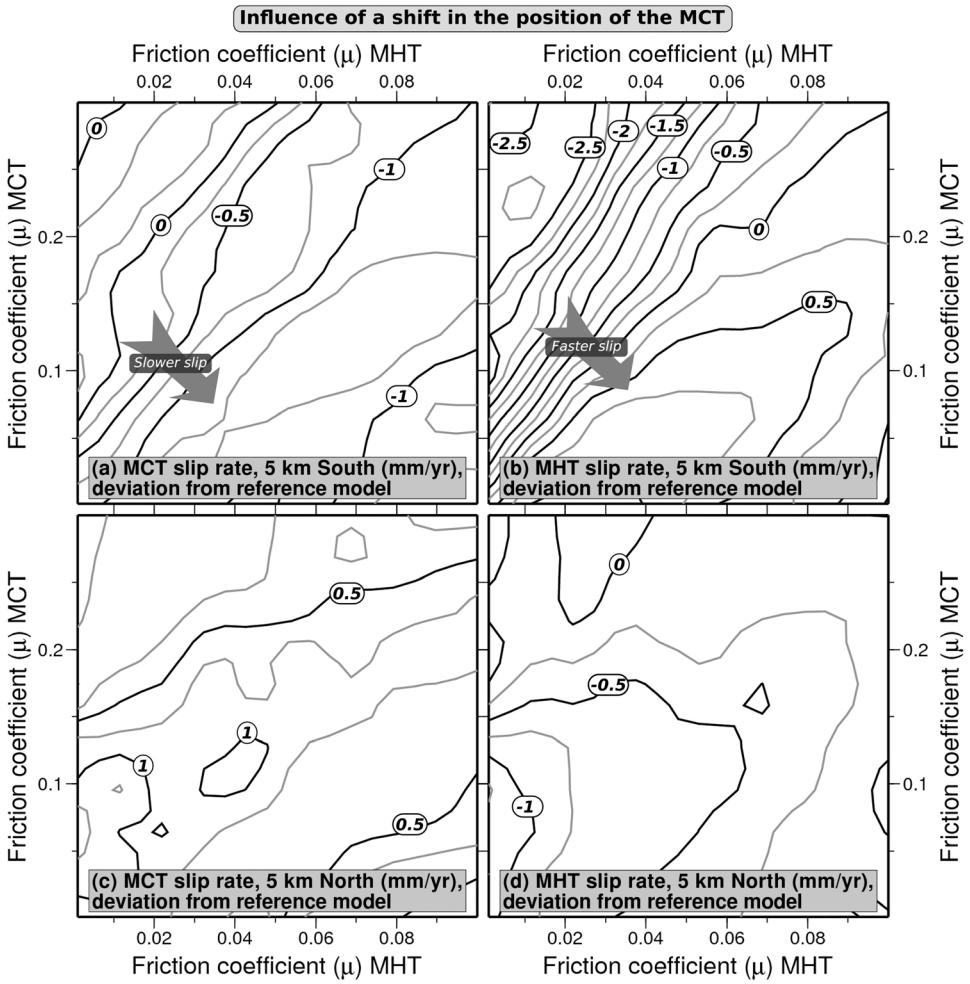

Figure 6. Influence of shifts in the north-south position of the MCT on the slip partitioning between the MCT and the MHT. The MCT is shifted ±5 km with respect to its position in the reference model. Contour lines indicate the deviation in slip rates (mm/yr) from the reference model (Figure 4). (a) Difference in slip rate on the MCT with respect to the reference model when shifting the MCT 5 km southward (Figure 4a). (b) Difference in slip rate on the MHT with respect to the reference model when shifting the MCT 5 km southward (Figure 4b). (c) Difference in slip rate on the MCT with respect to the reference model when shifting the MCT 5 km northward (Figure 4a). (d) Difference in slip rate on the MHT with respect to the reference model when shifting the MCT 5 km northward (Figure 4b). A southward shift of the MCT places it in a loading regime that is more similar to that of the MHT ramp, such that slip is inhibited on the MCT and transferred to the MHT.

stress changes modulate the Coulomb stress and promote or inhibit slip. The magnitude of normal and shear stresses is a direct function of the dip of the fault, such that fault dip becomes a major factor controlling the effective sensitivity to surface-load variations. For example, normal stress variations are likely to be significantly amplified on a gently dipping fault. The impact of loads on stresses typically also depend on the depth along the fault plane, on the magnitude of loading and unloading, and on the distance of the loaded area from the fault.

6.1. Large-Scale Erosion of the Topography

[33] For models in which no erosion is acting on the topographic surface versus the reference model, the absence of the modulating influence of erosion allows topography to grow quickly in areas of high rock uplift. The building of high topography above major ramps, such as along the MFT, leads to a negative feedback, whereby the mass of the relief creates an increasing resistance that counter-balances the tectonic forces and makes it harder to generate slip on the corresponding structure (Figure 7). Such slip-rate sensitivity to topographic loads is apparent on the MHT for low friction coefficients (Figure 7b): the development of the topography in the Siwaliks will tend to inhibit the slip on the MHT, whereas rapid erosion of the weakly cemented foreland strata in the MHT hanging wall [*Lavé and Avouac*, 2000] enables slip. A similar phenomenon exists on the MCT for high friction coefficients on the MHT (Figure 7a), i.e., in a situation where the MCT is more likely to accommodate a significant part of the convergence. On the other hand, when slip is slower on the MHT (for $\mu < 0.02$ on the MHT and $\mu > 0.15$ on the MCT: Figure 7b), the slip rate

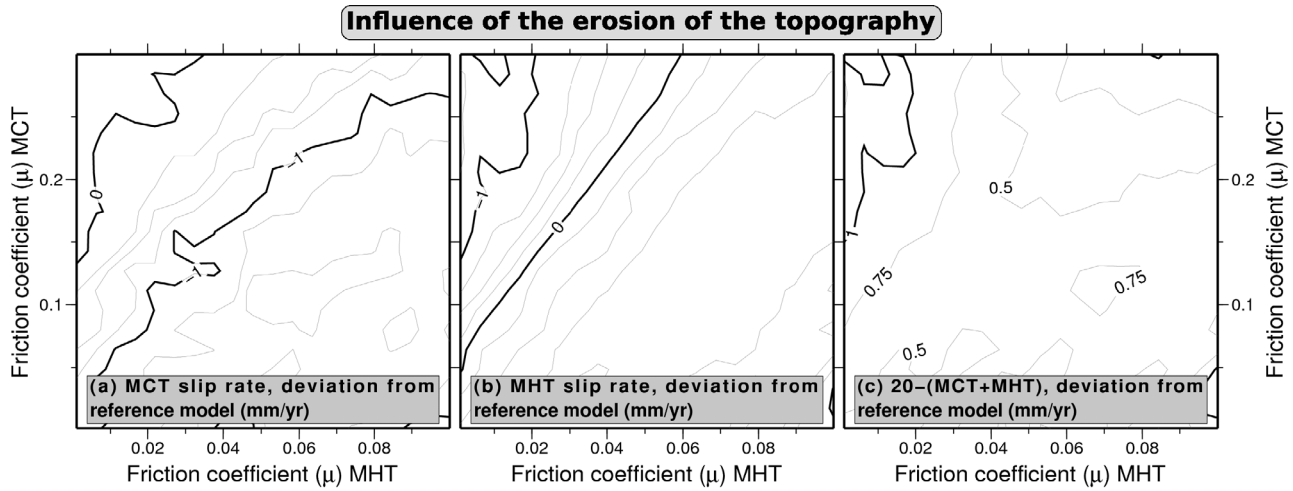

Figure 7. Influence of erosion of the topography on the activity of the faults and the slip partitioning between the MCT and the MHT. Contours show the difference between runs without erosion and the reference model (Figure 4). (a) Difference in slip rate on the MCT with respect to the reference model (Figure 4a). (b) Difference in slip rate on the MHT with respect to the reference model (Figure 4b). (c) Difference between the applied velocity (20 mm/yr) and the combined slip rates on the MCT and MHT, with respect to the reference model (Figure 4c).

on the MCT is not significantly different from the reference model (Figure 7a). Notably, these small changes indicate that the resulting deficit in slip on the MHT is not transferred to the MCT, but rather is accommodated as distributed deformation (Figure 7c).

6.2. Time-Varying Focused Erosion

[34] The models of the previous section were designed to provide general insights on the large-scale geodynamical impact of erosion, but do not explore the actual influence of shorter wavelength variations in erosion patterns that are likely to occur over several climatic cycles. As presented in section 2, erosion is expected to be highly variable with time in the high range due primarily to changes in glacial coverage and precipitation [*Duncan et al.*, 1998; *Pratt-Sitaula*, 2005; *Bookhagen et al.*, 2005a, 2005b; *Godard et al.*, 2011]. Here we present a series of simple sensitivity tests that aim at creating mechanical forcings similar to those resulting from fluctuations of glaciers in the High Himalaya.

[35] We model the influence of focused glacial erosion in the high range on fault slip (Figure 8). We use 0.01 and 0.15 for the friction coefficients of the MHT and MCT, respectively, because these values are consistent with observed slip rates (Figure 4). A uniform erosion window is applied across the High Himalaya and southernmost Tibetan Plateau (between 120 and 150 km as indicated on Figures 1c and 3) in addition to the background erosion of the topography. This additional focused erosion is modulated through time by a sine wave, with periods representing climatic cycles of 10 and 40 ky, that continuously allows the glacial erosion to sweep from 0 up to the maximal defined value. This periodicity creates pulsed, active unloading in the high range that is intended to explore the influence of episodic, rapid erosion by glaciers in an area which currently displays relatively low interglacial denudation rates [*Gabet et al.*, 2008].

[36] An increase in the intensity of glacial erosion induces a progressive acceleration of slip on the MCT and the development of larger finite slip than in the reference model (Figure 8b). For example, an erosion increase from ≤1 mm/yr (the modern observed interglacial rate: *Gabet et al.* [2008]) to 5 mm/yr (a permissible glacial rate) causes about a 30% increase in the fault slip rate (Figure 8b). This acceleration is an expression of the progressive unclamping of the MCT due to the unloading directly above the fault and the reduction of normal stresses. We note that time variations in the erosive forcing, i.e., the 10- or 40- ky modulating sine wave, are not temporally coupled with the slip on the MCT through time. This absence of a time-dependent response suggests that the system is more sensitive to the long-term cumulative effects of the unloading, rather than to the short-term variations in erosion. For the same erosion intensity, the response in terms of total slip on the MCT is apparently slightly higher with a 10-ky modulating period (Figure 8b), but this difference is actually due to a small difference in the cumulative erosion between the 10 and 40 ky forcings that appears during the onset of erosion in the simulation. In contrast to the MCT, the influence of the erosional unloading on the MHT slip is very limited (Figure 8a). If the eroding area is shifted progressively to the north by increments of 10 km, more distal positions for the glacial erosion with respect to the MCT induce a decrease in the finite slip accommodated on that fault (Figure 8c). This model result suggests a strong slip sensitivity to the position of the focused erosion with respect to the fault [*Hampel et al.*, 2009].

[37] Finally, we test the influence of combined spatial and temporal variations in erosion. Our aim is to test the influence of pulsed shifts of the locus of erosion such as those that might be associated with the alternation of glacial erosion in the high range during glacial periods with more active monsoon-driven erosion on the southern flank of the range during interglacials. To study the response of the model to this change in the site of maximum unloading, we consider two sites of focused erosion: (1) one area between 120 and 150 km (the high, glaciated Himalaya: Figure 1f)

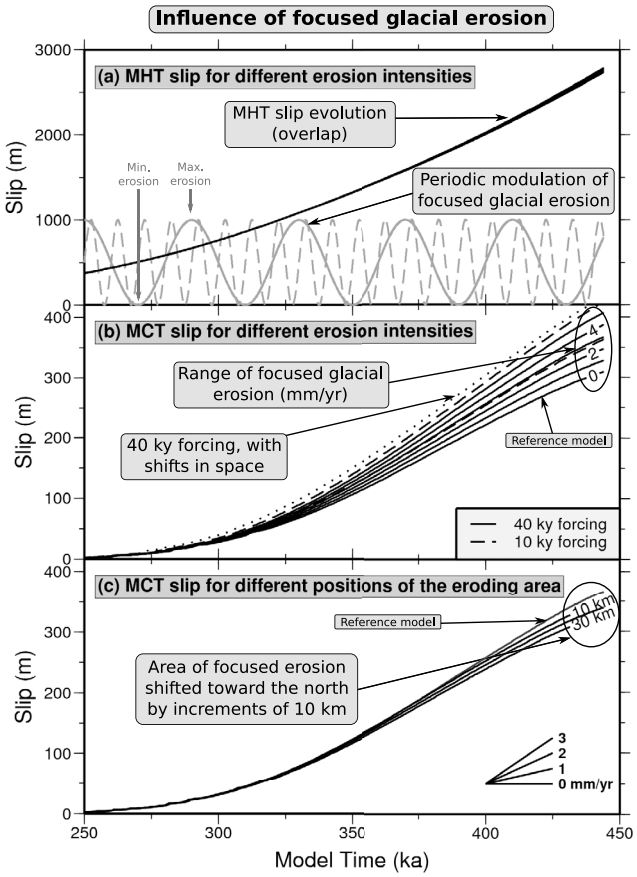

Figure 8. Influence of focused glacial erosion on slip activity of the MHT and MCT. The reference friction coefficients are 0.01 and 0.15 on the MHT and MCT, respectively. Erosion is applied between 120 and 150 km (Figure 3) and modulated by a sine wave with a 10- or 40-ky period, that makes glacial erosion fluctuate between 0 and the maximal defined value. (a) Influence on the MHT slip of different erosion intensities, ranging between 0 and 5 mm/yr. (b) Influence of different erosion intensities on the MCT slip. The solid lines indicate the response of the system to focused erosion ranging from 0 to 5 mm/yr by 1 mm/yr increments and modulated with 40-ky periods. The dashed lines refer to erosion intensity of 2 and 5 mm/yr and modulated with 10-ky periods. The dotted line corresponds to a more complex erosion pattern where focused erosion shifts from south to north and back over periods of 40 ky (see text for details), with a maximum value of 1 mm/yr in the south (90–120 km) and 2 mm/yr in the north(120–150 km). (c) Decreased slip due to shifting the erosion zone northward by 10, 20, and 30 km with respect to its reference position. Erosion intensity is 3 mm/yr.

where we impose an additional erosion oscillating between 0 and 2 mm/yr as in the previous models and (2) another one between 90 and 120 km (the monsoon-dominated Himalaya: Figure 1e) where we impose an additional erosion ranging from 0 to 1 mm/yr. Both forcings are modulated by a sine wave with a 40-ky period and are antiphased. We observe that, similar to our previous models, the oscillating nature of the forcing is not visible in the slip history of the MCT (Figure 8b, dotted curve). We also note that the finite slip is much higher than in the situation where only the northernmost "glacial" erosion is acting at the same maximum rate of 2 mm/yr. This increase is a consequence of the additional proximal unloading driven by monsoonal erosion directly above the MCT. These results support the concept that the MCT is mostly sensitive to the cumulative amount of erosion in the high range, rather than to its fine-scale distribution in space and time.

6.3. Influence of Ice Loads in the High Range

[38] In order to analyze the behavior of the system to loads that are more similar to those considered by previous studies [*Hetzel and Hampel*, 2005; *Turpeinen et al.*, 2008; *Hampel et al.*, 2009], we impose pressure loads in the high range between 120 and 150 km (Figures 1c and 3), that are equivalent to those imposed by 100 or 400 m of ice (Figures 4b and 9). This model scenario is designed to test the influence of the weight of shrinking and expending glaciers in the High Himalayas over the late Quaternary. We test two periods for the variations of the ice mass, corresponding to typical climatic variabilities of 10 and 40 ky, and we observe that the loading slows down the MCT, but that the frequency of the oscillations is either imperceptible or very modest in both cases, even with the maximum load of 400 m of ice. This decrease in the MCT slip rate due to ice loads is consistent with the mechanical explanation proposed by earlier studies, where such increased loads induce an increase in the normal stresses acting on the fault plane and tend to clamp the fault.

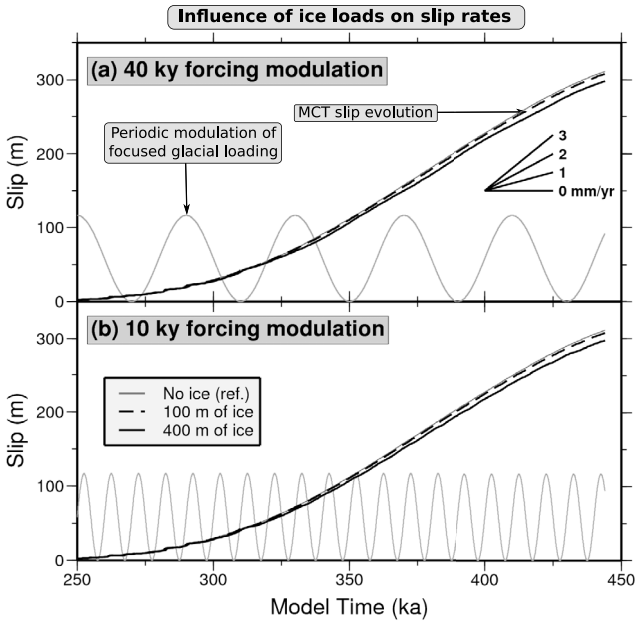

Figure 9. Influence of an ice load applied on the topography between 120 and 150 km and modulated by a sine wave with periods of 40 and 10 ky that makes the load fluctuate between 0 and the maximal imposed value (equivalent to either 100 or 400 m of ice). The reference friction coefficients are 0.01 and 0.15 on the MHT and MCT, respectively. The gray line is the reference model. The black dashed and solid lines are models where loads equivalent to 100 and 400 m of ice are applied, respectively.

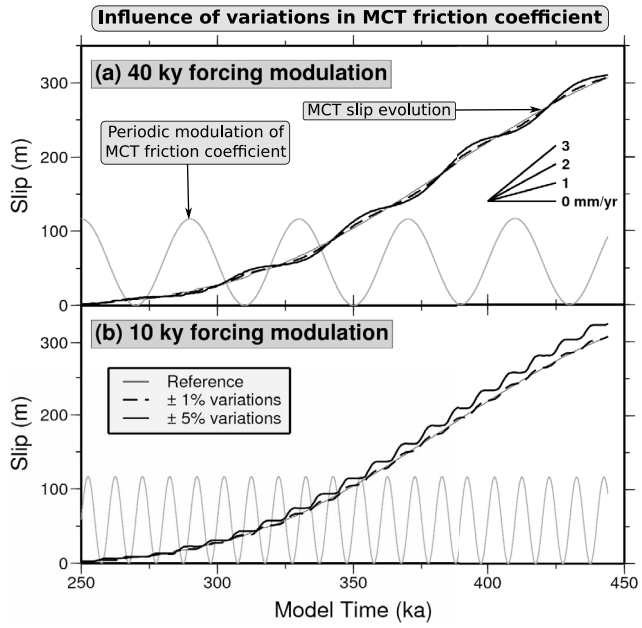

Figure 10. Slip variations on the MCT due to varying the friction coefficient for it. The reference friction coefficients are 0.01 and 0.15 on the MHT and MCT, respectively. The solid gray curve is the reference model (no variations of the coefficient with time). The dashed and solid gray lines are cases where the friction coefficient is modulated with a sine wave by ±2% and ±5% around the reference value, respectively. (a) 40-ky period for the modulation. (b) 10-ky period for the modulation.

[39] We note two main differences with respect to the conclusions of some previous workers, such as *Turpeinen et al.* [2008]. First, total suppression of slip does not occur at the height of the loading phase. As explained above, continued slip is a consequence of the much higher tectonic loading rates in our model. These rates prevail over external parameters in controlling the slip activity of the faults. Second, the slip deficit is not recovered during the unloading because slip has been transmitted to MHT, such that no stress accumulation results from the decrease in the slip rate of the MCT. In this sense, the ability to partition deformation between the MCT and MHT decreases the sensitivity of the MCT to surface loads.

[40] The 400-m value for the ice load is generally above the estimates for ice coverage over in the high range of central Nepal during the local Last Glacial Maximum [*Pratt-Sitaula*, 2005]. This upper bound, therefore, suggests that ice loading and unloading alone can not be a cause of significant modulation of the strain partitioning, although this conclusion is dependent on the values we use for the rheological parameters and reference friction coefficients. We predict that lower friction coefficients will induce a greater sensitivity of the system to external loads.

6.4. Time-Varying Friction Coefficients

[41] The MCT is a zone of intense fluid circulation, with a hydrothermal system closely connected to surface hydrology [*Derry et al.*, 2009], and it has been shown in other regions that meteoritic water could penetrate deep in the upper crust [*Craw et al.*, 1994]. We speculate that variations in water availability at the surface that are likely to be related to changing climatic conditions over time may be transmitted to the shallow parts of the MCT. This fluid flux would induce a change in physical conditions in the fault zone in terms of lubrication and pore pressure that could impact the effective friction. Although we acknowledge that the existence of such an effect can not be readily validated with the currently available geological and geophysical data, we nevertheless test several scenarios of friction coefficient variations for the MCT (Figure 10). Our aim here is to provide further insights on the mechanical sensitivity of the system to variations in its boundary conditions. Thus, we test the response of the orogen to oscillations in the friction coefficient of the MCT around its reference value with different periods that are typical of climatic times scales: 10 and 40 ky (Figure 10).

[42] For these different frequencies, small variations of the friction coefficient are directly expressed as significant slowing or acceleration of the slip rate on the MCT. The 40-ky oscillations with 5% changes in frictional coefficients induce about 50% changes in predicted slip rates (Figure 10a). In the case of the higher frequency oscillations (10 ky), the increase of the friction coefficient by only 5% results in a total suppression of slip, whereas a comparable reduction in the coefficient more than doubles the fault slip rate (Figure 10b). We also note that the 10-ky oscillations result in a finite slip at the end of the simulation that is significantly higher than in the reference model. This increase is a consequence of the temporary suppression of slip of the MCT that induces systematic overshooting when the fault is reactivated. This overshot only appears for the high frequency oscillations, which suggests that it results from the short-term accumulation of elastic energy in the deforming wedge, when the MCT is locked, that can not be efficiently dissipated by increasing the slip on the MHT. These simulations illustrate the idea that relatively small variations in the friction conditions on the fault plane could result in pronounced and geodynamically significant effects in terms of slip rate on crustal-scale faults at Milankovitch timescales.

7. Discussion

7.1. Implications for Himalayan Tectonics

[43] Our study presents a detailed and systematic analysis of the mechanical behavior of the MCT/MHT system in the Himalayas (Figure 11). Whereas some of the responses of the models to the various changes in boundary conditions that we have explored here can be intuited from simple considerations on the mechanical efficiency of the faults and minimum work principle, the systematic exploration of these responses allows derivation of useful quantitative information on the modalities of slip partitioning.

[44] Our models suggest that variations of the friction coefficients on either fault have major implications for the large-scale deformation pattern of the Himalayas. Strong frictional contrasts can induce highly contrasting kinematics, wherein either fault can act as the dominant structure for the accommodation of overall convergence. More importantly, we note that measured rates of Holocene slip impose strict bounds on the values of the friction coeffi-

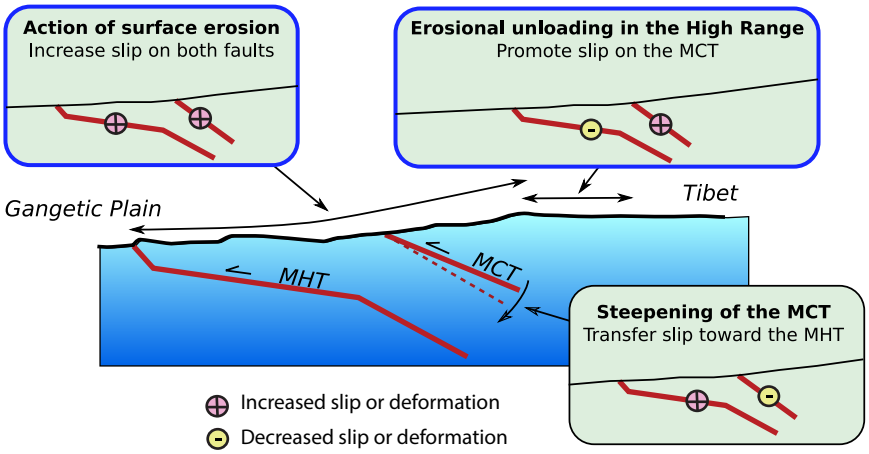
Action of surface erosion
Increase slip on both faults
Erosional unloading in the High Range
Promote slip on the MCT
Gangetic Plain
Tibet
MHT
MCT
Steepening of the MCT
Transfer slip toward the MHT
Increased slip or deformation
Decreased slip or deformation

et al., 2010a]. In contrast, farther west in the Marsyandi catchment, a localized offset in cooling ages exists (Figure 2) and has been used to propose reactivation of the MCT there [*Huntington et al.*, 2006; *Blythe et al.*, 2007], whereas a recent study by *Robert et al.* [2011] suggests that out-of-sequence reactivation is not required to explain the distribution of thermochronological ages in this region of the Marsyandi and Kali Gandaki. Clearly more data are needed to document the patterns of exhumation in the Himalayas Nepal and discriminate among the different models, but we propose that an understanding of the kinematic variability along the Himalayan arc should focus on variations in the dip of the structures as one of the primary explanatory parameters.

7.2. Influence of Surface Loads

[47] Several studies have already used generic models to investigate the influence of ice or erosional loading and unloading in modulating the slip of different types of faults [*Hampel and Hetzel*, 2006; *Turpeinen et al.*, 2008; *Maniatis et al.*, 2009]. Those studies have shown that, in the case of far-field extension or convergence rates of the order of 2 mm/yr, variations in surface loads could modulate the activity of the faults embedded in the model. One of the major differences between our modeling and those studies is that we impose a shortening velocity that mimics modern geodetic rates across the Himalaya and is an order of magnitude higher on the model domain. In this situation of faster and more intense tectonic processes, it might be expected that the relative impact of similar surface loads on fault activity is likely to be less pronounced and partly hidden behind the background tectonic signal. In our models, fault slip is primarily driven by the imposed horizontal stresses and the possible range of variations associated with modulation of vertical stresses is relatively narrow. We also note that the ice loads imposed in these previous studies are equivalent to several hundreds meters of ice, whereas we doubt that spatially averaged ice loads would exceed 100 m in the glaciated Himalaya due to the typical hillslope steepness (>20°). Thus, our study suggests that slip-rate modulation by glacial or erosional loads is likely to be less efficient in environments characterized by high rates of tectonic loading. Nonetheless, the fission track data [*Burbank et al.*, 2003; *Blythe et al.*, 2007] imply average erosion rates in the glacial-periglacial Himalayan realm have been significantly faster than those observed today. Our analysis suggests that increasing the erosion rate to 4 mm/yr (rates consistent with the fission track ages) from today's rate of 1 mm/yr would increase the magnitude of slip on the MCT by about 30% (Figure 8). However, even with such a significant increase in slip rate, erosional unloading alone appears insufficient to explain the full offset in cooling ages observed along the Marsyandi river (Figure 2).

[48] A clear sensitivity of fault zones to surface loads at shorter time-scales has also been highlighted by several previous workers [e.g., *Luttrell et al.*, 2007]. In particular, two recent studies have demonstrated that the tectonic regime of the Himalayas of central Nepal could display significant variations at annual timescales as a response to seasonal variations in surface loads. Using continuous GPS time series, *Bettinelli et al.* [2008] have shown that, across the range, the strain pattern with respect to a long-term trend displayed clear seasonal fluctuations, which they attributed to the cyclic loading of the Gangetic plain by monsoon rainwater. Similarly, from the investigation of microseismicity databases, *Bollinger et al.* [2007] demonstrated the existence of a statistically significant variation in the occurrence of Himalayan earthquakes between the winter and the summer. They also interpret the relative decrease of seismicity in the summer as a consequence of monsoon loads in the Himalayan foreland. Whereas these studies both deal with surface-loading processes at much shorter timescales than the ones we investigate here and activate different physical mechanisms, such as perturbations of the elastic interseismic strain field, they clearly demonstrate an elevated sensitivity of the Himalayan tectonic behavior to external perturbations. The processes presented by those two studies are by nature oscillatory and of low magnitude, but they ultimately tend to support the idea that infinitesimal and unidirectional unloading on an annual basis can result in a finite alteration of the tectonic deformation if it accumulates over the long term. This summation may lead to an excess or deficit in slip on major faults, such as that which we model for the MCT as a consequence of focused unloading in the High Himalaya (Figure 8).

7.3. Mechanical Behavior at Scales of a Fault or Orogenic Wedge

[49] In a similar modeling approach, *Cattin and Avouac* [2000] proposed that the friction coefficients could be up to 0.6 on the ramp of the MHT and up to 0.13 on the flat portion of this fault. These values are much higher than those we infer in our study for the Holocene kinematic configuration. This seeming inconsistency is a direct consequence of the possibility that, in our model, the mechanical system can transfer convergence to the MCT, if slip on the MHT is not energetically favorable. Such partitioning was not possible in Cattin and Avouac's model and apparently allowed higher friction coefficients on the MHT than are viable in our model. We note that the thermo-kinematic modeling approach proposed by *Herman et al.* [2010a] that considers friction-dependent shear heating on the main faults also leads to the conclusion that the friction coefficient needs to be low on the MHT.

[50] The range of the friction coefficients inferred for the MHT suggests a relatively weak fault (Figure 4), but is consistent with constraints derived for major continental crustal-scale faults in Tibet [*He and Chéry*, 2008], along the San Andreas fault zone [*Lachenbruch and Sass*, 1980; *Zoback and Beroza*, 1993; *Faulkner and Rutter*, 2001; *Parsons*, 2002] or in subduction zones [*Magee and Zoback*, 1993]. The contrast in friction coefficients between the MHT and MCT might be a consequence of the high availability of fluids along the MHT, derived from the metamorphism of sediments of the subducting Indian plate, as inferred from geophysical imaging [*Nabelek et al.*, 2009]. In contrast, whereas hydrothermal convection is intense in the MCT zone in the near surface [*Derry et al.*, 2009], its at-depth extension is speculative and is not observable with available geophysical data. Climatically driven fluid variability may only affect a rather superficial portion of the fault, may be buffered by a vigorous groundwater system, or may have no large-scale impact on fault friction and

behavior (Figure 10). However, the fact that very modest variations in friction coefficient can significantly modulate slip on the fault without being overridden by the background rates of tectonic loading suggests that intrinsic fault zone properties might need to be further considered when discussing the variability of fault slip rates over time.

[51] From a broader perspective, the causes of localization of deformation in active orogenic systems is one of the most important issues for our understanding of orogenic dynamics. Such a problem is often formulated in terms of energetic efficiency on the different faults that may accommodate deformation [*Cubas et al.*, 2008], and the system should tend to favor deformation scenarios that minimize the integrated amount of work required to cope with the far-field shortening, either by developing new structures, outward or inward, or by reactivating pre-existing faults. Our study is consistent with this minimum work principle, but also illustrates the idea that, in the case of a geometrically complex orogen, slight modifications of internal properties or boundary conditions can lead to substantial shifts in the deformation pattern and to evolutionary sequences that are either sustained or transient. Previous studies have highlighted some specific modes of evolution of orogenic wedges that develop in a changing climate [*Stolar et al.*, 2006; *Whipple and Meade*, 2006; *Whipple*, 2009], where the outward expansion of the range or reduction in its width are directly connected to changes in climatically controlled erosional efficiency. Most of these studies used critical wedge formulations [*Dahlen*, 1990] that do not allow assessment of how the strain response to the climatic forcing is distributed on discrete faults. On the other hand, our study introduces pre-defined fault zones as contact interfaces in the model (Figure 3), but does not allow for the development of new shortening zones during the simulation. Analog modeling approaches that allow for both localized deformation on fault-like structures, as well as dynamic development and abandonment of these structures, have highlighted a complex temporal evolution of orogenic wedge behavior [*Konstantinovskaia and Malavieille*, 2005; *Hoth et al.*, 2007], with complex cycles of fault activity and distribution of deformation across the wedge at climatic time-scales. The sensitivity of strain partitioning inside the wedge to variations in erosion that is illustrated by our study (Figure 8) and others [*Maniatis et al.*, 2009], suggests that the *internal clock* of *Hoth et al.* [2007] and forcing by fluctuating climate, especially when acting at similar time-scales, are probably intimately intertwined in dictating the actual tectonic evolution and changes in the distribution of deformation of active orogens.

7.4. Limitations and Future Research Directions

[52] We have used a simplified geometry for the contact interfaces intended as representations of the MCT and MHT in our numerical model, where they are modeled as a combination of straight-line segments. Although several arguments can be used to posit a flat/ramp geometry for the MHT in central Nepal [*Schelling and Arita*, 1991; *Pandey et al.*, 1995; *Lavé and Avouac*, 2001], the evolution of the MCT dip at depth remains unknown, and whether this structure becomes progressively gentler as it merges with a mid-crustal basal thrust is a question that still needs to be answered, possibly by high-resolution geophysical imagery [*Schulte-Pelkum et al.*, 2005; *Nabelek et al.*, 2009]. Nevertheless, we anticipate that variations at depth of the dip angle of the MCT, with respect to the reference dip of the upper part of the fault, will have similar effects on slip partitioning to that which was observed for the whole MCT in this study (Figure 5). Steepening at depth (i.e., formation of a ramp) will lead to slip transfer toward the MHT, but would probably be less pronounced because it will affect only part of the fault.

[53] Independently of the degree of complexity we assume for the faults, our sensitivity tests on the dip angle of the MCT (Figure 5) demonstrate that structural variations can have a first-order impact on the kinematics of the range. On the basis of those results, we argue that the fine-scale documentation of the along-strike variations in the geometry of both the MHT and MCT is probably one of the most important elements for understanding the kinematics of the Himalayan range at 10–100 ky time-scales.

[54] Our study was initially spurred by the intriguing temporal variations of erosion in the high range [*Burbank et al.*, 2003; *Gabet et al.*, 2008] and the sharp offset in cooling ages across the MCT zone [*Huntington et al.*, 2006; *Blythe et al.*, 2007] in the Marsyandi catchment. We acknowledge, however, that no unambiguous evidence exists for a significant Holocene activity of the MCT in that area, even if several data sets in adjacent areas point toward recent tectonic activity focused in the physiographic transition [*Wobus et al.*, 2003; *Hodges et al.*, 2004; *Wobus et al.*, 2005]. Decisive field evidence still needs to be provided to assess the existence and, if present, the magnitude of recent slip on the MCT. We note that recent developments in low-temperature thermochronology have made available new dating techniques with very low closure temperatures [*Herman et al.*, 2010b], that would have the potential to detect very recent and relatively small amplitude variations in exhumation across the MCT zone. Detailed geomorphic mapping in this steep, rapidly eroding, and monsoon-drenched southern flank of the High Himalayas is difficult but high-resolution analysis of stream profiles [*Craddock et al.*, 2007] and CRN inventories in stream sediments [*Wobus et al.*, 2005] also have the potential to yield other pieces of evidence.

8. Conclusions

[55] Strain partitioning between major shortening structures is a key feature of deformation within orogenic wedges. Whereas increasingly detailed documentation of fault slip rates can provide an overall kinematic picture of this process, the mechanical aspects of partitioning are still poorly resolved. In the Himalaya of central Nepal, the problem of slip partitioning between thrust faults, such as the Main Himalayan Thrust and the Main Central Thrust, is still actively debated. Whereas this problem has been previously explored using thermo-kinematic approaches [*Brewer and Burbank*, 2006; *Whipp et al.*, 2007; *Robert et al.*, 2009; *Herman et al.*, 2010a], no clear mechanical framework has been proposed that could provide a physical understanding of the partitioning between those two faults. Our study is an attempt to deliver this kind of perspective on the behavior of the range and should help the joint analysis

of the diversity of structural styles, geomorphologic controls, and kinematic regimes that are observed along the Himalayan belt.

[56] Various modes of interactions between tectonics and surface processes in active mountain ranges have been proposed over the last 20 years. Our study suggests the existence of an intriguing sensitivity of the Himalayan wedge to surface loads. In the context of background slip rates imposed by the far-field tectonic loading, our models indicate that reasonable unloading configurations could significantly modulate slip rates on major faults. Whereas such responses are dependent on the assumptions made for crustal rheology and fault strength, our results suggest the existence of significant transient adjustments at climatic time-scales (10–100 ky) such that the idea of tectonic steady state in an active mountain range should be used with caution and in a time frame that exceeds the scale of short-term variability.

[57] **Acknowledgments.** This research was funded by a Marie Curie Fellowship (Geocycl-219662) to V.G. and by NSF (EAR 0819874) and NASA (NNX08AG05G) grants to D.W.B. The authors acknowledge the support of the Institute of Crustal Studies and, in particular, Chen Ji for access to computational facilities. We thank B. Bookhagen, G. B. Fisher, and J.-P. Avouac for helpful discussions during the development of this project. Constructive comments by Frédéric Herman, Peter van der Beek, Associate Editor W. P. Schellart, and one anonymous reviewer helped to improve this manuscript.

References

Armijo, R., P. Tapponnier, J. L. Mercier, and H. Tong-Lin (1986), Quaternary extension in southern Tibet: Field observations and tectonic implications, *J. Geophys. Res.*, *91*, 13,803–13,872, doi:10.1029/JB091iB14p13803.

Armstrong, R., B. Raup, S. Khalsa, R. Barry, J. Kargel, C. Helm, and H. Kieffer (2005), Glims glacier database, *Tech. rep.*, Natl. Snow and Ice Data Cent., Boulder, Colo.

Avouac, J.-P. (2003), Mountain building, erosion, and the seismic cycle in the Nepal Himalaya, *Adv. Geophys.*, *46*, 1–80.

Avouac, J.-P. (2007), Dynamic processes in extensional and compressional settings–Mountain building: From earthquakes to geological deformation, in *Treatise of Geophysics*, vol. 6, *Crust and Lithosphere Dynamics*, edited by A. B. Watts, pp. 377–439, Elsevier, Boston, doi:10.1016/B978-044452748-6.00112-7.

Avouac, J.-P., and E. B. Burov (1996), Erosion as a driving mechanism of intracontinental mountain growth, *J. Geophys. Res.*, *101*, 17,747–17,770, doi:10.1029/96JB01344.

Beaumont, C., P. Fullsack, and J. Hamilton (1992), Erosional control of active compressional orogens, in *Thrust Tectonics*, vol. 99, pp. 1–18, Chapman and Hall, London.

Beaumont, C., R. A. Jamieson, M. H. Nguyen, and B. Lee (2001), Himalayan tectonics explained by extrusion of a low-viscosity crustal channel coupled to focused surface denudation, *Nature*, *414*, 738–742, doi:10.1038/414738a.

Berger, A. L., et al. (2008), Quaternary tectonic response to intensified glacial erosion in an orogenic wedge, *Nat. Geosci.*, *1*, 793–799, doi:10.1038/ngeo334.

Bettinelli, P., J. Avouac, M. Flouzat, F. Jouanne, L. Bollinger, P. Willis, and G. Chitrakar (2006), Plate motion of India and interseismic strain in the Nepal Himalaya from GPS and DORIS measurements, *J. Geod.*, *80*(8), 567–589, doi:10.1007/s00190-006-0030-3.

Bettinelli, P., J. Avouac, M. Flouzat, L. Bollinger, G. Ramillien, S. Rajaure, and S. Sapkota (2008), Seasonal variations of seismicity and geodetic strain in the Himalaya induced by surface hydrology, *Earth Planet. Sci. Lett.*, *266*, 332–344, doi:10.1016/j.epsl.2007.11.021.

Bilham, R., K. M. Larson, and J. T. Freymueller (1997), GPS measurements of present-day convergence across the Nepal Himalaya, *Nature*, *386*, 61–64, doi:10.1038/386061a0.

Blythe, A., D. Burbank, A. Carter, K. Schmidt, and J. Putkonen (2007), Plio-Quaternary exhumation history of the central Nepalese Himalaya: 1. Apatite and zircon fission track and apatite [U-Th]/He analyses, *Tectonics*, *26*, TC3002, doi:10.1029/2006TC001990.

Bollinger, L., J. P. Avouac, O. Beyssac, E. J. Catlos, T. M. Harrison, M. Grove, B. Goffé, and S. Sapkota (2004a), Thermal structure and exhumation history of the Lesser Himalaya in central Nepal, *Tectonics*, *23*, TC5015, doi:10.1029/2003TC001564.

Bollinger, L., J. P. Avouac, R. Cattin, and M. R. Pandey (2004b), Stress buildup in the Himalaya, *J. Geophys. Res.*, *109*, B11405, doi:10.1029/2003JB002911.

Bollinger, L., F. Perrier, J. P. Avouac, S. Sapkota, U. Gautam, and D. R. Tiwari (2007), Seasonal modulation of seismicity in the Himalaya of Nepal, *Geophys. Res. Lett.*, *34*, L08304, doi:10.1029/2006GL029192.

Bookhagen, B., and D. W. Burbank (2006), Topography, relief, and TRMM-derived rainfall variations along the Himalaya, *Geophys. Res. Lett.*, *33*, L08405, doi:10.1029/2006GL026037.

Bookhagen, B., R. C. Thiede, and M. R. Strecker (2005a), Late Quaternary intensified monsoon phases control landscape evolution in the northwest Himalaya, *Geology*, *33*(2), 149–152.

Bookhagen, B., R. C. Thiede, and M. R. Strecker (2005b), Abnormal monsoon years and their control on erosion and sediment flux in the high, arid northwest Himalaya, *Earth Planet. Sci. Lett.*, *231*, 131–146.

Brewer, I. D., and D. W. Burbank (2006), Thermal and kinematic modeling of bedrock and detrital cooling ages in the central Himalaya, *J. Geophys. Res.*, *111*, B09409, doi:10.1029/2004JB003304.

Brewer, I. D., D. W. Burbank, and K. V. Hodges (2006), Downstream development of a detrital cooling-age signal: Insights from 40Ar/39Ar muscovite thermochronology in the Nepalese Himalaya, in *Tectonics, Climate, and Landscape Evolution*, edited by S. D. Willett et al., *Spec. Pap. Geol. Soc. Am.*, *398*, 321–338.

Burbank, D. W., A. E. Blythe, J. Putkonen, B. Pratt-Sitaula, E. Gabet, M. Oskin, A. Barros, and T. P. Ojha (2003), Decoupling of erosion and precipitation in the Himalayas, *Nature*, *426*, 652–655, doi:10.1038/nature02187.

Calais, E., A. M. Freed, R. Van Arsdale, and S. Stein (2010), Triggering of New Madrid seismicity by late-Pleistocene erosion, *Nature*, *466*, 608–611, doi:10.1038/nature09258.

Carter, N. L., and M. C. Tsenn (1987), Flow properties of continental lithosphere, *Tectonophysics*, *136*(1–2), 27–63, doi:10.1016/0040-1951(87)90333-7.

Catlos, E., T. M. Harrison, M. Kohn, M. Grove, M. Ryerson, C. E. Manning, and B. N. Upreti (2001), Geochronologic and thermobarometric constraints on the evolution of the Main Central Thrust, central Nepal Himalaya, *J. Geophys. Res.*, *106*, 16,177–16,204, doi:10.1029/2000JB900375.

Cattin, R., and J. P. Avouac (2000), Modeling mountain building and the seismic cycle in the Himalaya of Nepal, *J. Geophys. Res.*, *105*, 13,389–13,407, doi:10.1029/2000JB900032.

Cattin, R., G. Martelet, P. Henry, J.-P. Avouac, M. Diament, and T. R. Shakya (2001), Gravity anomalies, crustal structure and thermo-mechanical support of the Himalaya of central Nepal, *Geophys. J. Int.*, *147*(2), 381–392, doi:10.1046/j.0956-540x.2001.01541.x.

Craddock, W. H., D. W. Burbank, B. Bookhagen, and E. J. Gabet (2007), Bedrock channel geometry along an orographic rainfall gradient in the upper Marsyandi River valley in central Nepal, *J. Geophys. Res.*, *112*, F03007, doi:10.1029/2006JF000589.

Craw, D., P. O. Koons, D. Winslow, C. P. Chamberlain, and P. Zeitler (1994), Boiling fluids in a region of rapid uplift, Nanga Parbat massif, Pakistan, *Earth Planet. Sci. Lett.*, *128*, 169–182, doi:10.1016/0012-821X(94)90143-0.

Cubas, N., Y. M. Leroy, and B. Maillot (2008), Prediction of thrusting sequences in accretionary wedges, *J. Geophys. Res.*, *113*, B12412, doi:10.1029/2008JB005717.

Dahlen, F. (1990), Critical taper model of fold-and-thrust belts and accretionary wedges, *Annu. Rev. Earth Planet. Sci.*, *18*(1), 55–99.

DeCelles, P., D. Robinson, J. Quade, T. Ojha, C. Garzione, P. Copeland, and B. Upreti (2001), Stratigraphy, structure, and tectonic evolution of the Himalayan fold-thrust belt in western Nepal, *Tectonics*, *20*(4), 487–509, doi:10.1029/2000TC001226.

Derry, L. A., M. J. Evans, R. Darling, and C. France-Lanord (2009), Hydrothermal heat flow near the Main Central Thrust, central Nepal Himalaya, *Earth Planet. Sci. Lett.*, *286*, 101–109, doi:10.1016/j.epsl.2009.06.036.

Duncan, C. C., A. J. Klein, J. G. Masek, and B. L. Isacks (1998), Comparison of Late Pleistocene and modern glacier extents in central Nepal based on digital elevation data and satellite imagery, *Quat. Res.*, *49*(3), 241–254, doi:10.1006/qres.1998.1958.

Faulkner, D. R., and E. H. Rutter (2001), Can the maintenance of overpressured fluids in large strike-slip fault zones explain their apparent weakness?, *Geology*, *29*(6), 503–506.

Friedrich, A. M., B. P. Wernicke, N. A. Niemi, R. A. Bennett, and J. L. Davis (2003), Comparison of geodetic and geologic data from the

Wasatch region, Utah, and implications for the spectral character of Earth deformation at periods of 10 to 10 million years, *J. Geophys. Res.*, *108*(B4), 2199, doi:10.1029/2001JB000682.

Fuller, C. W., S. D. Willett, and M. T. Brandon (2006), Formation of forearc basins and their influence on subduction zone earthquakes, *Geology*, *34*(2), 65–68, doi:10.1130/G21828.1.

Gabet, E. J., B. A. Pratt-Sitaula, and D. W. Burbank (2004a), Climatic controls on hillslope angle and relief in the Himalayas, *Geology*, *32*(7), 629–632.

Gabet, E. J., D. W. Burbank, J. K. Putkonen, B. A. Pratt-Sitaula, and T. Ojha (2004b), Rainfall thresholds for landsliding in the Himalayas of Nepal, *Geomorphology*, *63*(3–4), 131–143, doi:10.1016/j.geomorph.2004.03.011.

Gabet, E. J., D. W. Burbank, B. Pratt-Sitaula, J. Putkonen, and B. Bookhagen (2008), Modern erosion rates in the High Himalayas of Nepal, *Earth Planet. Sci. Lett.*, *267*, 482–494, doi:10.1016/j.epsl.2007.11.059.

Gabet, E. J., D. Wolff-Boenisch, H. Langner, D. W. Burbank, and J. Putkonen (2010), Geomorphic and climatic controls on chemical weathering in the High Himalayas of Nepal, *Geomorphology*, *122*(1–2), 205–210, doi:10.1016/j.geomorph.2010.06.016.

Gansser, A. (1964), *Geology of the Himalayas*, vol. 289, Interscience, London.

Garzanti, E., G. Vezzoli, S. Andò, J. Lavé, M. Attal, C. France-Lanord, and P. DeCelles (2007), Quantifying sand provenance and erosion (Marsyandi River, Nepal Himalaya), *Earth Planet. Sci. Lett.*, *258*, 500–515, doi:10.1016/j.epsl.2007.04.010.

Gayer, E., J. Lavé, R. Pik, and C. France-Lanord (2006), Monsoonal forcing of Holocene glacier fluctuations in Ganesh Himal (central Nepal) constrained by cosmogenic 3He exposure ages of garnets, *Earth Planet. Sci. Lett.*, *252*, 275–288, doi:10.1016/j.epsl.2006.09.040.

Godard, V., R. Cattin, and J. Lavé (2004), Numerical modeling of mountain building: Interplay between erosion law and crustal rheology, *Geophys. Res. Lett.*, *31*, L23607, doi:10.1029/2004GL021006.

Godard, V., J. Lavé, and R. Cattin (2006), Numerical modelling of erosion processes in the Himalayas of Nepal: Effects of spatial variations of rock strength and precipitation, in *Analogue and Numerical Modelling of Crustal-Scale Processes*, edited by S. J. H. Buiter and G. Schreurs, *Geol. Soc. Spec. Publ.*, *253*, 341–358, doi:10.1144/GSL.SP.2006.253.01.18.

Godard, V., R. Cattin, and J. Lavé (2009), Erosional control on the dynamics of low-convergence rate continental plateau margins, *Geophys. J. Int.*, *179*(2), 763–777, doi:10.1111/j.1365-246X.2009.04324.x.

Godard, V., D. W. Burbank, D. L. Bourlès, B. Bookhagen, R. Braucher, and G. B. Fisher (2011), Constraining catchment-scale glacial erosion using a global inversion of detrital CRN data in the Himalayas of central Nepal, in *Geophys. Res. Abstr.*, *13*, EGU2011-1447.

Goodbred, S. L., and S. A. Kuehl (1999), Holocene and modern sediment budgets for the Ganges-Brahmaputra river system: Evidence for highstand dispersal to flood-plain, shelf, and deep-sea depocenters, *Geology*, *27*(6), 559–562.

Hampel, A., and R. Hetzel (2006), Response of normal faults to glacial-interglacial fluctuations of ice and water masses on Earth's surface, *J. Geophys. Res.*, *111*, B06406, doi:10.1029/2005JB004124.

Hampel, A., R. Hetzel, and A. L. Densmore (2007), Postglacial slip-rate increase on the Teton normal fault, northern Basin and Range Province, caused by melting of the Yellowstone ice cap and deglaciation of the Teton Range?, *Geology*, *35*(12), 1107–1110.

Hampel, A., R. Hetzel, G. Maniatis, and T. Karow (2009), Three-dimensional numerical modeling of slip rate variations on normal and thrust fault arrays during ice cap growth and melting, *J. Geophys. Res.*, *114*, B08406, doi:10.1029/2008JB006113.

Harper, J. T., and N. F. Humphrey (2003), High altitude Himalayan climate inferred from glacial ice flux, *Geophys. Res. Lett.*, *30*(14), 1764, doi:10.1029/2003GL017329.

Harrison, T. M., M. Grove, O. M. Lovera, and E. J. Catlos (1998), A model for the origin of Himalayan anatexis and inverted metamorphism, *J. Geophys. Res.*, *103*, 27,017–27,032.

Hassani, R., D. Jongmans, and J. Chéry (1997), Study of plate deformation and stress in subduction processes using two-dimensional numerical models, *J. Geophys. Res.*, *102*, 17,951–17,966, doi:10.1029/97JB01354.

He, J., and J. Chéry (2008), Slip rates of the Altyn Tagh, Kunlun and Karakorum faults (Tibet) from 3D mechanical modeling, *Earth Planet. Sci. Lett.*, *274*, 50–58, doi:10.1016/j.epsl.2008.06.049.

Henry, P., X. Le Pichon, and B. Goffé (1997), Kinematic, thermal and petrological model of the Himalayas: Constraints related to metamorphism within the underthrust Indian crust and topographic elevation, *Tectonophysics*, *273*(1–2), 31–56, doi:10.1016/S0040-1951(96)00287-9.

Herman, F., et al. (2010a), Exhumation, crustal deformation, and thermal structure of the Nepal Himalaya derived from the inversion of thermochronological and thermobarometric data and modeling of the topography, *J. Geophys. Res.*, *115*, B06407, doi:10.1029/2008JB006126.

Herman, F., E. J. Rhodes, J. Braun, and L. Heiniger (2010b), Uniform erosion rates and relief amplitude during glacial cycles in the Southern Alps of New Zealand, as revealed from OSL-thermochronology, *Earth Planet. Sci. Lett.*, *297*, 183–189, doi:10.1016/j.epsl.2010.06.019.

Hetényi, G., R. Cattin, J. Vergne, and J. L. Nábělek (2006), The effective elastic thickness of the India Plate from receiver function imaging, gravity anomalies and thermomechanical modelling, *Geophys. J. Int.*, *167*(3), 1106–1118, doi:10.1111/j.1365-246X.2006.03198.x.

Hetzel, R., and A. Hampel (2005), Slip rate variations on normal faults during glacial–interglacial changes in surface loads, *Nature*, *435*, 81–84, doi:10.1038/nature03562.

Hodges, K. V. (2000), Tectonics of the Himalaya and southern Tibet from two perspectives, *Geol. Soc. Am. Bull.*, *112*(3), 324–350.

Hodges, K. V., J. M. Hurtado, and K. X. Whipple (2001), Southward extrusion of Tibetan crust and its effect on Himalayan tectonics, *Tectonics*, *20*(6), 799–809.

Hodges, K. V., C. Wobus, K. Ruhl, T. Schildgen, and K. Whipple (2004), Quaternary deformation, river steepening, and heavy precipitation at the front of the Higher Himalayan ranges, *Earth Planet. Sci. Lett.*, *220*, 379–389, doi:10.1016/S0012-821X(04)00063-9.

Hoth, S., A. Hoffmann-Rothe, and N. Kukowski (2007), Frontal accretion: An internal clock for bivergent wedge deformation and surface uplift, *J. Geophys. Res.*, *112*, B06408, doi:10.1029/2006JB004357.

Huntington, K. W., and K. V. Hodges (2006), A comparative study of detrital mineral and bedrock age-elevation methods for estimating erosion rates, *J. Geophys. Res.*, *111*, F03011, doi:10.1029/2005JF000454.

Huntington, K. W., A. E. Blythe, and K. V. Hodges (2006), Climate change and Late Pliocene acceleration of erosion in the Himalaya, *Earth Planet. Sci. Lett.*, *252*, 107–118, doi:10.1016/j.epsl.2006.09.031.

Jouanne, F., J. L. Mugnier, M. R. Pandey, J. F. Gamond, P. Le Fort, L. Serrurier, C. Vigny, and J. P. Avouac (1999), Oblique convergence in the Himalayas of western Nepal deduced from preliminary results of GPS measurements, *Geophys. Res. Lett.*, *26*(13), 1933–1936, doi:10.1029/1999GL900416.

Kirby, S. H. (1983), Rheology of the lithosphere, *Rev. Geophys.*, *21*(6), 1458–1487.

Kirby, S. H., and A. K. Kronenberg (1987), Rheology of the lithosphere: Selected topics, *Rev. Geophys.*, *25*(6), 1219–1244.

Konstantinovskaia, E., and J. Malavieille (2005), Erosion and exhumation in accretionary orogens: Experimental and geological approaches, *Geochem. Geophys. Geosyst.*, *6*, Q02006, doi:10.1029/2004GC000794.

Lachenbruch, A. H., and J. H. Sass (1980), Heat flow and energetics of the San Andreas fault zone, *J. Geophys. Res.*, *85*, 6185–6222, doi:10.1029/JB085iB11p06185.

Larson, K. M., R. Bürgmann, R. Bilham, and J. T. Freymueller (1999), Kinematics of the India-Eurasia collision zone from GPS measurements, *J. Geophys. Res.*, *104*, 1077–1094, doi:10.1029/1998JB900043.

Lavé, J., and J. Avouac (2000), Active folding of fluvial terraces across the Siwaliks Hills, Himalayas of central Nepal, *J. Geophys. Res.*, *105*, 5735–5770, doi:10.1029/1999JB900292.

Lavé, J., and J. P. Avouac (2001), Fluvial incision and tectonic uplift across the Himalayas of central Nepal, *J. Geophys. Res.*, *106*, 26,561–26,591, doi:10.1029/2001JB000359.

Le Fort, P. (1975), Himalayas: the collided range. Present knowledge of the continental arc, *Am. J. Sci.*, *275*(1), 1–44.

Leloup, P. H., G. Mahéo, N. Arnaud, E. Kali, E. Boutonnet, D. Liu, L. Xiaohan, and L. Haibing (2010), The south Tibet detachment shear zone in the dinggye area: Time constraints on extrusion models of the Himalayas, *Earth Planet. Sci. Lett.*, *292*, 1–16, doi:10.1016/j.epsl.2009.12.035.

Luttrell, K., D. Sandwell, B. Smith-Konter, B. Bills, and Y. Bock (2007), Modulation of the earthquake cycle at the southern San Andreas fault by lake loading, *J. Geophys. Res.*, *112*, B08411, doi:10.1029/2006JB004752.

Lyon-Caen, H., and P. Molnar (1985), Gravity anomalies, flexure of the Indian plate and the structure, support and evolution of the Himalaya and Ganga Basin, *Tectonics*, *4*(6), 513–538.

Magee, M. E., and M. D. Zoback (1993), Evidence for a weak interplate thrust fault along the northern Japan subduction zone and implications for the mechanics of thrust faulting and fluid expulsion, *Geology*, *21*(9), 809–813.

Maniatis, G., D. Kurfeß, A. Hampel, and O. Heidbach (2009), Slip acceleration on normal faults due to erosion and sedimentation—Results from a new three-dimensional numerical model coupling tectonics and landscape evolution, *Earth Planet. Sci. Lett.*, *284*, 570–582, doi:10.1016/j.epsl.2009.05.024.

Martin, A. J., P. G. DeCelles, G. E. Gehrels, P. J. Patchett, and C. Isachsen (2005), Isotopic and structural constraints on the location of the Main

Central Thrust in the Annapurna Range, central Nepal Himalaya, *Geol. Soc. Am. Bull.*, *117*(7–8), 926–944.
Martin, A. J., J. Ganguly, and P. G. DeCelles (2010), Metamorphism of Greater and Lesser Himalayan rocks exposed in the Modi Khola valley, central Nepal, *Contrib. Mineral. Petrol.*, *159*(2), 203–223, doi:10.1007/s00410-009-0424-3.
Nabelek, J., G. Hetenyi, J. Vergne, S. Sapkota, B. Kafle, M. Jiang, H. Su, J. Chen, B.-S. Huang, and Hi-CLIMB Team (2009), Underplating in the Himalaya-Tibet collision zone revealed by the Hi-CLIMB experiment, *Science*, *325*(5946), 1371–1374, doi:10.1126/science.1167719.
Owen, L. A., and D. I. Benn (2005), Equilibrium-line altitudes of the Last Glacial Maximum for the Himalaya and Tibet: An assessment and evaluation of results, *Quat. Int.*, *138*, 55–78, doi:10.1016/j.quaint.2005.02.006.
Owen, L. A., R. C. Finkel, and M. W. Caffee (2002), A note on the extent of glaciation throughout the Himalaya during the global Last Glacial Maximum, *Quat. Sci. Rev.*, *21*(1–3), 147–157, doi:10.1016/S0277-3791(01)00104-4.
Owen, L. A., M. W. Caffee, R. C. Finkel, and Y. B. Seong (2008), Quaternary glaciation of the Himalayan-Tibetan orogen, *J. Quat. Sci.*, *23*(6–7), 513–531, doi:10.1002/jqs.1203.
Pandey, M. R., R. P. Tandukar, J.-P. Avouac, J. Lave, and J.-P. Massot (1995), Interseismic strain accumulation on the Himalayan crustal ramp (Nepal), *Geophys. Res. Lett.*, *22*(7), 751–754, doi:10.1029/94GL02971.
Parsons, T. (2002), Nearly frictionless faulting by unclamping in long-term interaction models, *Geology*, *30*(12), 1063–1066.
Pearson, O. N., and P. G. DeCelles (2005), Structural geology and regional tectonic significance of the Ramgarh thrust, Himalayan fold-thrust belt of Nepal, *Tectonics*, *24*, TC4008, doi:10.1029/2003TC001617.
Pratt, B., D. W. Burbank, A. Heimsath, and T. Ojha (2002), Impulsive alluviation during early Holocene strengthened monsoons, central Nepal Himalaya, *Geology*, *30*(10), 911–914.
Pratt-Sitaula, B. (2005), Glaciers, climate, and topography in the Nepalese Himalaya, Ph.D. thesis, Univ. of Calif., Santa Barbara.
Rahaman, W., S. K. Singh, R. Sinha, and S. K. Tandon (2009), Climate control on erosion distribution over the Himalaya during the past 100 ka, *Geology*, *37*(6), 559–562, doi:10.1130/G25425A.1.
Robert, X., P. van der Beek, J. Braun, C. Perry, M. Dubille, and J. L. Mugnier (2009), Assessing Quaternary reactivation of the Main Central Thrust zone (central Nepal Himalaya): New thermochronologic data and numerical modeling, *Geology*, *37*(8), 731–734, doi:10.1130/G25736A.1.
Robert, X., P. van der Beek, J. Braun, C. Perry, and J.-L. Mugnier (2011), Control of detachment geometry on lateral variations in exhumation rates in the Himalaya: Insights from low-temperature thermochronology and numerical modeling, *J. Geophys. Res.*, *116*, B05202, doi:10.1029/2010JB007893.
Robinson, D. M., P. G. DeCelles, C. N. Garzione, O. N. Pearson, T. M. Harrison, and E. J. Catlos (2003), Kinematic model for the Main Central thrust in Nepal, *Geology*, *31*(4), 359–362.
Schelling, D. (1992), The tectonostratigraphy and structure of the eastern Nepal Himalaya, *Tectonics*, *11*(5), 925–943, doi:10.1029/92TC00213.
Schelling, D., and K. Arita (1991), Thrust tectonics, crustal shortening, and the structure of the far-eastern Nepal Himalaya, *Tectonics*, *10*(5), 851–862, doi:10.1029/91TC01011.
Scherler, D., B. Bookhagen, and M. R. Strecker (2011), Spatially variable response of Himalayan glaciers to climate change affected by debris cover, *Nat. Geosci.*, *4*, 156–159, doi:10.1038/ngeo1068.
Schulte-Pelkum, V., G. Monsalve, A. Sheehan, M. R. Pandey, S. Sapkota, R. Bilham, and F. Wu (2005), Imaging the Indian subcontinent beneath the Himalaya, *Nature*, *435*, 1222–1225, doi:10.1038/nature03678.
Searle, M. P., and L. Godin (2003), The South Tibetan detachment and the Manaslu Leucogranite: A structural reinterpretation and restoration of the Annapurna-Manaslu Himalaya, Nepal, *J. Geol.*, *111*, 505–523, doi:10.1086/376763.
Searle, M. P., R. Law, L. Godin, K. Larson, M. Streule, J. Cottle, and M. Jessup (2008), Defining the Himalayan Main Central Thrust in Nepal, *J. Geol. Soc.*, *165*(2), 523–534, doi:10.1144/0016-76492007-081.
Stolar, D. B., S. D. Willett, and G. H. Roe (2006), Climatic and tectonic forcing of a critical orogen, in *Tectonics, Climate, and Landscape Evolution*, edited by S. D. Willett et al., *Spec. Pap. Geol. Soc. Am.*, *398*, 241–250.
Thiede, R. C., B. Bookhagen, J. R. Arrowsmith, E. R. Sobel, and M. R. Strecker (2004), Climatic control on rapid exhumation along the Southern Himalayan Front, *Earth Planet. Sci. Lett.*, *222*, 791–806, doi:10.1016/j.epsl.2004.03.015.
Tomkin, J. H., and G. H. Roe (2007), Climate and tectonic controls on glaciated critical-taper orogens, *Earth Planet. Sci. Lett.*, *262*, 385–397, doi:10.1016/j.epsl.2007.07.040.
Tsenn, M. C., and N. L. Carter (1987), Upper limits of power law creep of rocks, *Tectonophysics*, *136*(1–2), 1–26, doi:10.1016/0040-1951(87)90332-5.
Turpeinen, H., A. Hampel, T. Karow, and G. Maniatis (2008), Effect of ice sheet growth and melting on the slip evolution of thrust faults, *Earth Planet. Sci. Lett.*, *269*, 230–241, doi:10.1016/j.epsl.2008.02.017.
Underwood, P. (1983), Dynamic relaxation, in *Computational Methods for Transient Analysis*, vol. 1, pp. 245–265, North Holland, Amsterdam.
Wessel, P., and W. H. F. Smith (1991), Free software helps map and display data, *Eos Trans. AGU*, *72*(441), 445–446.
Whipp, D. M., T. A. Ehlers, A. E. Blythe, K. W. Huntington, K. V. Hodges, and D. W. Burbank (2007), Plio-Quaternary exhumation history of the central Nepalese Himalaya: 2. Thermokinematic and thermochronometer age prediction model, *Tectonics*, *26*, TC3003, doi:10.1029/2006TC001991.
Whipple, K. X. (2009), The influence of climate on the tectonic evolution of mountain belts, *Nat. Geosci.*, *2*, 97–104, doi:10.1038/ngeo413.
Whipple, K. X., and B. J. Meade (2006), Orogen response to changes in climatic and tectonic forcing, *Earth Planet. Sci. Lett.*, *243*, 218–228, doi:10.1016/j.epsl.2005.12.022.
Willett, S. (1999), Orogeny and orography: The effects of erosion on the structure of mountain belts, *J. Geophys. Res.*, *104*(B12), 28,957–28,981, doi:10.1029/1999JB900248.
Wobus, C. W., K. V. Hodges, and K. X. Whipple (2003), Has focused denudation sustained active thrusting at the Himalayan topographic front?, *Geology*, *31*(10), 861–864, doi:10.1130/G19730.1.
Wobus, C., A. Heimsath, K. X. Whipple, and K. Hodges (2005), Active out-of-sequence thrust faulting in the central Nepalese Himalaya, *Nature*, *434*, 1008–1011, doi:10.1038/nature03499.
Yin, A. (2006), Cenozoic tectonic evolution of the Himalayan orogen as constrained by along-strike variation of structural geometry, exhumation history, and foreland sedimentation, *Earth Sci. Rev.*, *76*(1–2), 1–131, doi:10.1016/j.earscirev.2005.05.004.
Zhang, P. Z., et al. (2004), Continuous deformation of the Tibetan Plateau from global positioning system data, *Geology*, *32*(9), 809–812, doi:10.1130/G20554.1.
Zhao, W., K. D. Nelson, J. Che, J. Quo, D. Lu, C. Wu, and X. Liu (1993), Deep seismic reflection evidence for continental underthrusting beneath southern Tibet, *Nature*, *366*, 557–559, doi:10.1038/366557a0.
Zoback, M. D., and G. C. Beroza (1993), Evidence for near-frictionless faulting in the 1989 (M 6.9) Loma Prieta, California, earthquake and its aftershocks, *Geology*, *21*(2), 181–185.

D. W. Burbank, Earth Research Institute, 6832 Ellison Hall, University of California, Santa Barbara, CA 93106-3060, USA.
V. Godard, CEREGE, CNRS, UMR 6635, Aix-Marseille Université, Europôle Méditerranéen de l'Arbois, BP 80, F-13290 Aix-en-Provence, France. (godard@cerege.fr)